



Spatial variation of seismogenic depths of crustal earthquakes in the Taiwan region: Implications for seismic hazard assessment



Wen-Nan Wu^{a,*}, Yin-Tung Yen^b, Ya-Ju Hsu^c, Yih-Min Wu^d, Jing-Yi Lin^{a,e}, Shu-Kun Hsu^{a,e}

^a Center for Environmental Studies, National Central University, No. 300, Zhongda Road, Zhongli District, Taoyuan City 32001, Taiwan

^b Sinotech Engineering Consultants, Inc., No. 280, Xinhua 2nd Road, Neihu District, Taipei City 11494, Taiwan

^c Institute of Earth Sciences, Academia Sinica, No. 128, Sec. 2, Academia Road, Nangang District, Taipei City 11529, Taiwan

^d Department of Geosciences, National Taiwan University, No. 1, Sec. 4, Roosevelt Road, Daan District, Taipei City 10617, Taiwan

^e Department of Earth Sciences, National Central University, No. 300, Zhongda Road, Zhongli District, Taoyuan City 32001, Taiwan

ARTICLE INFO

Article history:

Received 15 November 2016

Received in revised form 18 April 2017

Accepted 25 April 2017

Available online 26 April 2017

Keywords:

Seismogenic zone

Taiwan orogenic belt

Seismic hazard assessment

ABSTRACT

This paper presents the first whole Taiwan-scale spatial variation of the seismogenic zone using a high-quality crustal seismicity catalog. The seismicity onset and cutoff depths (i.e., seismogenic depths) are determined by the earthquake depth–moment distribution and used to define the upper and lower boundaries of the seismogenic zone, respectively. Together with the published fault geometries and fault area–moment magnitude relations, the depth difference in the onset and cutoff depths (i.e., seismogenic thickness) is used as the fault width to determine the moment magnitudes of potential earthquakes for the major seismogenic faults. Results show that the largest ($M_w 7.9$ – 8.0) potential earthquake may occur along the Changhua fault in western Taiwan, where the seismic risk is relatively high and seismic hazard mitigation should be a matter of urgent concern. In addition, the first-motion focal mechanism catalog is used to examine the relation between the seismogenic depths and earthquake source parameters. For crustal earthquakes (≤ 50 km), the shallowest onset and cutoff depths are observed for normal and strike-slip events, respectively. This observation is different from the prediction of the conventional continental-rheology model, which states that thrust events have the shallowest cutoff depth. Thus, a more sophisticated rheology model is necessary to explain our observed dependence of the seismogenic depths on faulting types. Meanwhile, for intermediate to large crustal ($M_w \geq 4$; depth ≤ 50 km) earthquakes, thrust events tend to occur at the bottom region of the seismogenic zone, but normal and strike-slip events distribute at a large depth range.

© 2017 Elsevier B.V. All rights reserved.

1. Introduction

Taiwan is located in an oblique convergent zone at a plate boundary, where the Philippine Sea Plate subducts northward beneath the Ryukyu Arc, while the Eurasia Plate subducts eastward beneath the Luzon Arc. A relative plate convergence at a rate of approximately 8 cm/yr along an azimuth of $N50^\circ W$ (e.g., DeMets et al., 2010; Yu et al., 1997) generates numerous earthquakes and complex geological features in Taiwan (Fig. 1). Here, we only briefly introduce the regional geology of Taiwan; a more detailed description has been presented in Ho (1986). As shown in Fig. 1, the geological structures of Taiwan generally trend NNE–SSW, and the prominent geological provinces from west to east are as follows (Ho, 1986): (1) the Coastal Plain, the present-day foreland basin; (2) the Western Foothills, comprising accreted and deformed sediments in the foreland basin; (3) the Hsuehshan Range, comprising a thick sequence of Eocene and Oligocene sedimentary rocks; (4) the Backbone

Range, composed of Miocene to Eocene slates; (5) the Eastern Central Range, the pre-Tertiary basement of the continental margin; (6) the Longitudinal Valley, the suture between the Eurasia and Philippine Sea plates; and (7) the Coastal Range, the compressed Luzon Arc and its forearc. Two small volcanic islands of Luta and Lanyu in the southeastern offshore are remnant Neogene island arc. In addition, two prominent tectonic structures, the Peikang High (PH) and the Lukang Magnetization High (LMH), are located in western Taiwan. The former presents the shallow pre-Cretaceous Chinese continental basement (Lin and Watts, 2002), and the latter could be viewed as a zone of relatively rigid crust (Hsu et al., 2008). These tectonic structures have been suggested to dominate earthquake occurrence and stress distribution in western Taiwan (Hsu et al., 2008; Hu et al., 1997; Lin, 2001; Wu et al., 2010).

During the last century, Taiwan has experienced serious damage from several destructive earthquakes inland and offshore (e.g., Ma and Liang, 2008; Shin and Teng, 2001; Wang, 1998) (Fig. 1), indicating that the unique tectonic setting of Taiwan is capable of accumulating a large amount of elastic strain that produces large earthquakes. Thus, it

* Corresponding author.

E-mail address: wennan@ncu.edu.tw (W.-N. Wu).

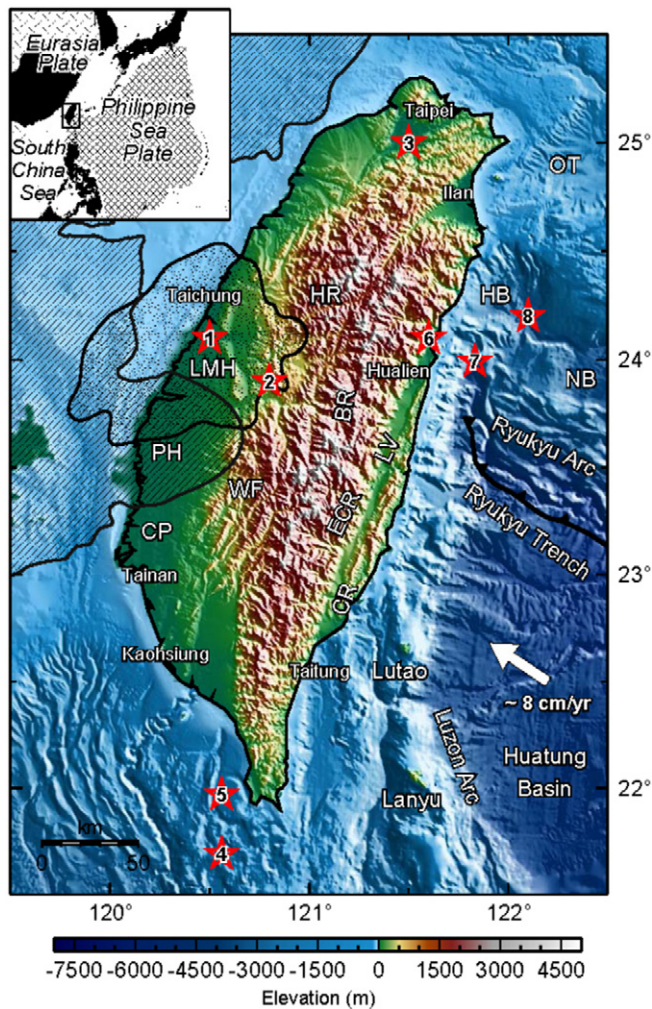


Fig. 1. Tectonic setting (inset) and major geologic units of the Taiwan region. CP: Coastal Plain; WF: West Foothill; HR: Hsueshan Range; BR: Backbone Range; ECR: East Coastal Range; LV: Longitudinal Valley; CR: Costal Range; HB: Hoping Basin; NB: Nanao Basin; RT: Ryukyu Trench; RTST: Ryukyu Taiwan Stress Transition; LMH: Lukang Magnetization High; PH: Peigan High. Open stars are disastrous earthquakes mentioned in the context. 1: the 1848 $M_{7.1}$ Changhua earthquake; 2: the 1999 $M_{w}7.6$ Chi-Chi earthquake; 3: the 1694 M_7 Taipei earthquake; 4: the 2006 M_7 Pingtung earthquake (first event); 5: the 2006 M_7 Pingtung earthquake (second event); 6: the May 1986 $M_{s6.3}$ Hualien earthquake; 7: the November 1986 $M_{s7.8}$ Hualien earthquake; 8: the 2002 $M_{w}7.0$ Hualien earthquake.

is critical to specifically assess the seismic hazard for the whole Taiwan region. For a successful seismic hazard assessment, the fundamental step is to determine potential moment magnitudes (M_w) of future large earthquakes on distinctive seismogenic structures.

The moment magnitude of an earthquake is proportional to the rupture area, which is the product of the rupture length and width (depth extent), of a brittle fault (Hanks and Kanamori, 1979; Kanamori and Anderson, 1975). Hence, it is critical to accurately determine the lengths and widths of seismogenic faults for the determination of moment magnitudes. However, the fault width is more difficult to define than the fault length, and only a few segments of active faults in Taiwan have been delineated by the reflection method (e.g., Wang et al., 2001; Wang et al., 2003; Wang et al., 2004; Wang et al., 2002). Due to a lack of a complete and reliable database of fault width for the active faults in Taiwan, previous studies have estimated the maximum magnitudes of future earthquake events (e.g., Cheng, 2002; Cheng et al., 2010; Shyu et al., 2005a) and the probability of seismic hazard (e.g., Cheng, 2002; Cheng et al., 2010; Lee, 2004) by assuming a constant rupture width (mostly 15 km) and a rupture length constrained from

geologically mapped active faults. To achieve a more accurate seismic hazard model, a more realistic estimation of the rupture width with lateral variations is required, which will in turn improve the estimation of moment magnitudes of potential earthquakes on any particular fault or seismic source.

In addition, a profusion of observations and simulations have suggested that buried-rupture earthquakes generate stronger near-fault ground motion than surface-rupturing earthquakes (e.g., Dalguer et al., 2008; Kagawa et al., 2004; Somerville, 2003). These studies have led to the adoption of a depth-dependence rupture model in next-generation ground-motion predictions (Power et al., 2008). It is widely accepted that the inclusion of the depth-to-top rupture extent in a strong motion simulation is crucial for seismic hazard mitigation. Unfortunately, the spatial distribution of the top edge of rupture faulting in the Taiwan region has not been delineated.

The seismogenic zone is generally defined as the earth's layer where earthquakes occur at depths, and the thickness of the seismogenic zone (seismogenic thickness, ST) is defined as the depth interval between the upper and lower boundaries of the seismogenic zone. These boundaries are reasonably assumed as proxies for the top and bottom edges of fault ruptures, respectively. The lower boundary of the seismogenic zone, above which a large percentage of earthquakes occur, is termed the seismicity "cutoff depth" (SCD) (Sibson, 1982). Similarly, the upper boundary of the seismogenic zone, where earthquakes begin to occur, is termed the seismicity "onset depth" (SOD). For the sake of conciseness, hereafter both SCD and SOD are referred to as the seismogenic depths. Furthermore, the seismogenic depths and the ST are termed as the seismogenic parameters.

A large number of studies have analyzed the earthquake depth-frequency distributions to determine the SCD in California and Japan (e.g., Bonner et al., 2003; Doser and Kanamori, 1986; Ito, 1990; Magistrale, 2002; Omuralieva et al., 2012; Sibson, 1982; Tanaka and Ishikawa, 2002; Williams, 1996). In Taiwan, Wang et al. (1994) and Ma and Song (2004) used the earthquake depth-frequency distribution to determine the SCD. Nevertheless, their study areas are limited and the resolution in their results may not be well constrained because of a relatively large uncertainty in the hypocenters from the seismicity catalogs they used. Wang et al. (1994) also suggested that earthquake faulting type is the second dominator in controlling seismicity depth in the Taiwan region. However, such a conclusion was drawn on the basis of investigation of limited regions with fewer data and less quantitative analysis for focal mechanism solutions. In addition, although a number of studies have reported that moderate to large earthquakes tend to occur near the bottom of the seismogenic zone (e.g., Das and Scholz, 1983; Ito, 1990; Sibson, 1982; Sibson, 1984; Yang et al., 2012), this relation is still unclear for Taiwan.

In this study, we first use an updated relocation seismicity catalog to determine the spatial distributions of the seismogenic parameters for the whole Taiwan region. Then, the high-resolution ST is used to determine the most likely magnitude of future events for major seismogenic faults in Taiwan and evaluate associated seismic potentials with recently published results. Finally, we explore relations between the seismogenic depths and source parameters of intermediate to large crustal earthquakes. Our results not only provide critical parameters for the seismic hazard evaluation but also shed new light on seismogenic behaviors of crustal earthquakes.

2. Data and analysis

2.1. Relocated seismicity catalog

An accurate and complete earthquake dataset will guarantee determination of reliable spatial distribution of the seismogenic zone from background seismicity. In our analysis, we use a well-relocated seismicity catalog containing data between 1990 and 2015, which is obtained by applying a 3D ray-tracing method (Um and Thurber, 1987) with

the station correction terms (Wu et al., 2003) and a 3D velocity model (Wu et al., 2009a) to a comprehensive travel-time dataset from the Taiwan Central Weather Bureau Seismic Network (CWBSN), Taiwan Strong Motion Instrumentation Program (TSMIP), Japan Meteorological Agency (JMA), and eleven one-week ocean bottom seismometers (Wu et al., 2009a; Wu et al., 2009b). This 3D relocated seismicity catalog not only minimizes the uncertainties from 3D structures but also represents a significant improvement over the general CWBSN catalog, which is located using a 1D velocity model (Chen and Shin, 1998), and other previous relocated catalogs that cover limited areas (e.g., Kim et al., 2005; Ma et al., 1996; Rau and Wu, 1995). Moreover, by using the same 3D velocity model and the earthquake location algorithm, ten explosion sites were relocated to examine earthquake location uncertainty. The relocation results show that the average location error in depth is 3.8 km (Wu et al., 2013), which is smaller than the grid space (5.0 km) used for the analysis in this study. This demonstrates that the used velocity model and relocation method can provide a reliable relocated seismicity catalog that can be used for subsequent analysis.

To further reduce uncertainties in the determination of the seismogenic depths, the poorly located events must be eliminated from the 3D relocated seismicity catalog. A conservative way is to use the most rigorous criteria to select events; however, this reduces the amount of available data, which decreases spatial resolution and increases uncertainties owing to small sample sizes. Maximizing data availability is essential when the aim is to determine seismogenic depths based on statistic inferences. Therefore, to maximize available high-quality data, we remove the events that have a vertical location uncertainty greater than the focal depth, a zero value for either vertical or horizontal location uncertainty, and an average value of vertical and horizontal location uncertainties exceeding 10 km (Gourley et al., 2007).

2.2. Crustal seismicity

On the basis of the filtered 3D relocated seismicity catalog, we select the crustal earthquakes that are constrained by the recently determined Moho geometry of Taiwan from teleseismic receiver function analysis (Wang et al., 2010a). In practice, we first adopt the Moho depths determined from the clear Moho P-to-S conversions for 27 permanent three-component broadband stations that were widely installed in the Taiwan region (Wang et al., 2010a). Subsequently, we interpolate the discrete locations with the Moho depths to construct a Moho model with 1-km resolution for the entire study area using minimum curvature splines (Wessel and Smith, 1998) (Fig. 2a). We adopt a value of 5 km into considering the uncertainties of the Moho depth and the earthquake focal depth, and the events located above the Moho discontinuity are considered as crustal earthquakes. In this case, the earthquakes related to the subducted slab at larger depths are expected to be eliminated, but the interplate earthquakes offshore of eastern and southwestern Taiwan may still dominate the determination of seismogenic depths. Three representative profiles across Taiwan show no significant correlation between the distributions of the Moho depth and the hypocenters (Fig. 2b, c, and d), indicating that the determination of seismogenic depths is independent of the Moho model. A total of 431,067 relocated earthquakes are available in this crustal earthquake catalog (Fig. 3a), and the average horizontal and vertical location uncertainties with one standard deviation (1σ) are 0.3 ± 0.3 and 0.3 ± 0.4 km, respectively.

2.3. Completeness of crustal seismicity catalog

According to the empirical relations between the earthquake magnitude and fault dimensions (e.g., Wells and Coppersmith, 1994), a $M_w 6$ earthquake may correspond to a fault length of about 10 km. To appropriately represent the fault geometry of intermediate and large ($M_w \geq 6$) earthquakes, we divide our study area into 0.05° -spacing grid nodes and include all events within a $0.05^\circ \times 0.05^\circ$ rectangle centered at the node.

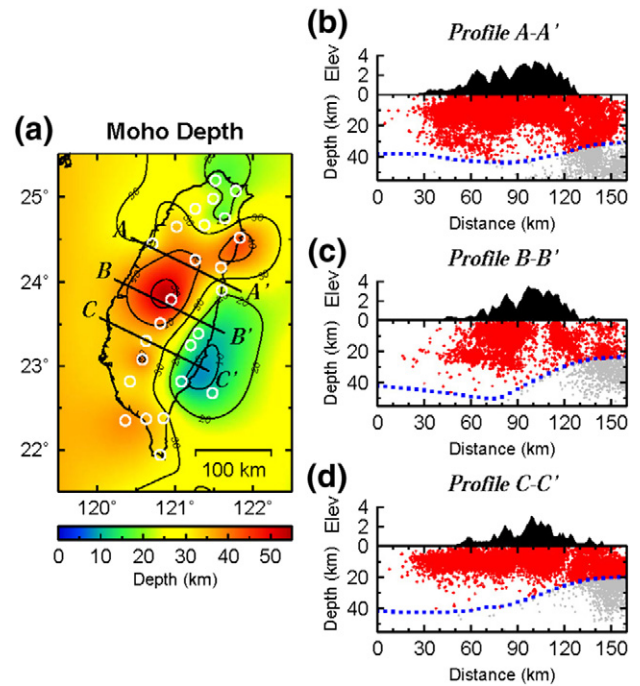


Fig. 2. (a) Spatial variation of the Moho depths derived from teleseismic receiver function analysis. The white circles are the locations of the broadband stations used to compute the Moho depths. Note that the station KMNB located at 24.46°N and 118.39°E is not shown here but used to constrain the Moho geometry. Three hypocenter projections (A–A', B–B' and C–C') are shown in (b), (c) and (d), respectively, to reveal the relations between the Moho geometry and relocated hypocenters. Background seismicity and crustal earthquakes within ± 5 km of each profile are represented by gray dots and red crosses. Dotted blue lines delineate the Moho depth. The A–A' and C–C' profiles correspond to the central and southern cross-island high ways, and the B–B' profile is the southern limit of exhumation of the Hsueshan Range along the Choushui river.

The number of earthquakes belonging to each grid node is shown in Fig. 3a; most grid nodes have > 100 events which is empirically sufficient for further statistics analysis.

To obtain robust results with statistical significance, the dataset must be complete, consistent, and homogeneous prior to determining seismogenic depths (Woessner and Wiemer, 2005). We calculate the minimum completeness magnitude (M_c) of the crustal earthquake catalog for each grid node with at least 30 events. M_c is defined as the lowest magnitude above which all earthquakes are reliably recorded by a seismic network (Rydelek and Sacks, 1989). The value of M_c may change with time and space (e.g., Hutton et al., 2010; Woessner and Wiemer, 2005), but the potential temporal variation is ignored.

We calculate M_c using the maximum curvature method, in which the point of maximum curvature is defined as M_c by computing the value of the first derivative of the frequency–magnitude curve (Wiemer and Wyss, 2000). Moreover, a bootstrap method is applied to calculate the mean value and its 1σ uncertainty of M_c for each grid node (e.g., Schorlemmer et al., 2003; Woessner and Wiemer, 2005). The mean estimate considers the uncertainties of the magnitude determination process, which can effectively eliminate the effect of the outliers (Woessner and Wiemer, 2005). In practice, we draw all events (at least 30 earthquakes) in each grid node, and allow any event to be selected more than once. This procedure is repeated 2000 times for the whole dataset and 1000 times for every grid node. The mean value and its 1σ uncertainty of M_c for the whole dataset are 2.10 and 0.01; these values for each grid node are shown in Fig. 3b and c, respectively. The M_c in offshore areas is generally larger than that in the mid-southern region, which is related to the seismic station coverage and reflects the seismicity-detected capability of seismic networks. On the basis of the distribution of M_c , we establish a complete and homogeneous seismicity catalog for the subsequent analysis.

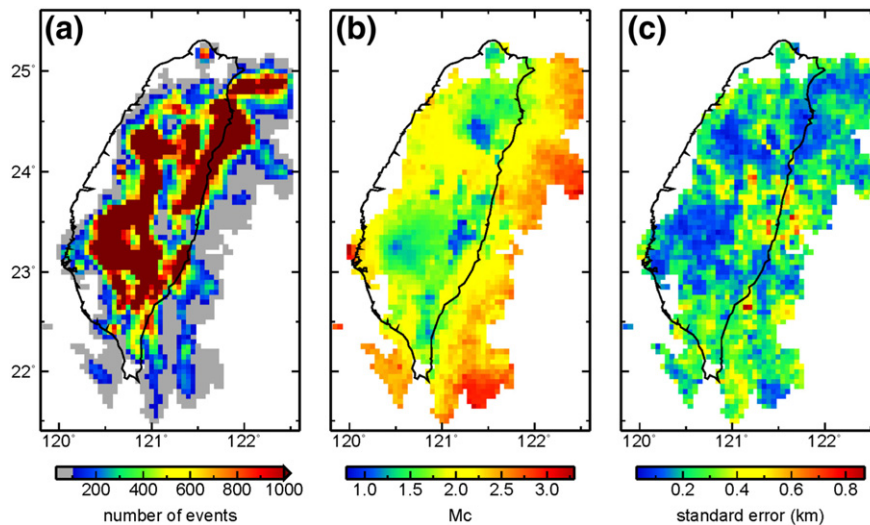


Fig. 3. (a) The number of crustal earthquakes at each grid cell. (b) Spatial variation in the magnitude of completeness (M_c) with errors using the bootstrap method shown in (c).

2.4. Determination of seismogenic depths and thickness

As described in Section 1, for crustal earthquakes, the SCD has been widely determined by the earthquake depth-frequency distribution, but the SOD has been paid little attention. In contrast, for the subduction zones, the updip and downdip limits of the interplate seismogenic zone were generally delineated by the distribution of interplate thrust earthquakes (e.g., Kao, 1998; Kao and Chen, 1991; Kao et al., 1998; Pacheco et al., 1993; Seno, 2005), seismicity/aftershocks distribution (e.g., Hippchen and Hyndman, 2008; Newman et al., 2002; Tilmann et al., 2010), extent of large earthquake coseismic slip (e.g., Chlieh et al., 2007; Oleskevich et al., 1999), and interseismic locked regions (e.g., Hashimoto et al., 2009; Schwartz and DeShon, 2007). A more recent study used the global earthquake catalogs to determine 5% and 95% of the interplate earthquake depth-frequency distribution along the interplate seismogenic zone and to define its updip and downdip limits for all subduction zones (Heuret et al., 2011). In this study, we follow an approach similar to that of Heuret et al. (2011) to use the widely accepted concept of presenting the seismogenic zone by earthquakes with depth in order to determine the SOD and SCD. However, we use the earthquake depth-moment accumulation with the different selected percentage values based on the following two concerns.

First, it is well known that the number of earthquakes exponentially emphasizes small earthquakes whose seismic moments are orders of magnitude less than those of large to moderate-sized events (Chen et al., 2012; Nazareth and Hauksson, 2004). It is practically unavoidable to include sub-crustal earthquakes in our crustal seismicity catalog. Thus, using the number of earthquakes to determine the seismogenic depths may introduce bias into the estimate of the seismogenic parameters. On the other hand, the seismic moment is not only physically clear but also directly linked to seismic strain release (Chen et al., 2012; Chen and Molnar, 1977; Kostrov, 1974). Therefore, we prefer to use the earthquake depth-moment accumulation instead of earthquake depth-frequency distribution for the determination of seismogenic depths. To compute the seismic moment release, the seismic moment (M_0 , dyne-cm) is converted from the local magnitude (M_L) through the relation $\log(M_0) = 1.27M_L + 17.23$, proposed by Chen et al. (2007). We disregard the uncertainty in the magnitude conversion because a large number of earthquakes are used in the conversion.

The second concern in the determination of seismogenic depths is how much percentage value of the earthquake depth-moment release distribution shall be used to determine seismogenic depths. In the literature, the percentage value of the earthquake depth-frequency distribution used to determine the SCD has been determined somewhat

arbitrarily. For example, the value of the maximum percentage for the determination of the SCD has ranged from 90% (Miller and Furlong, 1988; Omuralieva et al., 2012; Richards-Dinger and Shearer, 2000; Tanaka et al., 2004), to 95% (Ma and Song, 2004; Magistrale, 2002; Smith-Konter et al., 2011; Williams, 1996), to 99% (Bonner et al., 2003; Uski et al., 2012). To our best knowledge, no conclusive method is available to determine the optimal maximum percentage value of earthquake depth-frequency distribution or earthquake depth-moment accumulation for estimating seismogenic depths. Therefore, we take the depths of 1% (D_1), 5% (D_5), and 10% (D_{10}) as well as 90% (D_{90}), 95% (D_{95}), and 99% (D_{99}) from the moment release-depth-integrated beam as the upper (SOD) and lower (SCD) boundaries of the seismogenic zone, respectively. The ST is then determined by the depths from 1% to 99% (D_1 –99), from 5% to 95% (D_5 –95), and from 10% to 90% (D_{10} –90) of the cumulative moment release with depths. The spatial variation of the seismogenic parameters under the above definition is non-uniform. In addition, we use 1000 bootstrap resamples to obtain the mean values and 1σ uncertainties of the SOD, SCD, and ST for the entire data and for each grid node. To make our presentation clearer and more concise, only the results of D_{10} , D_{90} , and D_{10} –90 are discussed in the following sections and other results with different thresholds are displayed in Supplement Figs. S1–S3.

In addition, we determine the spatial distributions of D_{10} , D_{90} , and D_{10} –90 by the earthquake depth-frequency relation (Fig. S4), and compare them with that from the earthquake depth-moment accumulation (Fig. S5). Even though the differences in seismogenic parameters estimated from the two methods are minor (≤ 0.1 km on average), we still favor the results inferred from the earthquake depth-moment accumulation relation because of its physical meaning and insensitivity to the number of earthquakes considered.

3. Spatial variation of the seismogenic zone

3.1. Spatial variation of the upper boundary of the seismogenic zone

The distribution of the SOD (D_{10}) underneath the Taiwan region is at a depth of 1.1–32.0 km, and its mean value with the 1σ uncertainty is 6.7 ± 4.6 km (Fig. 4). As far as we know, a global survey of the SOD for crustal earthquakes is not available. For a regional scale, Ito (1999) reported that the SOD in southwest Japan is in the range 0.5–8 km, which agrees with the mean values (3.2–6.7 km) of our SOD (D_1 , D_5 , and D_{10}) estimates. In contrast, several global studies have estimated the updip limit of the interplate seismogenic zone. For example, an earlier study of seismic coupling along the subduction seismogenic zones

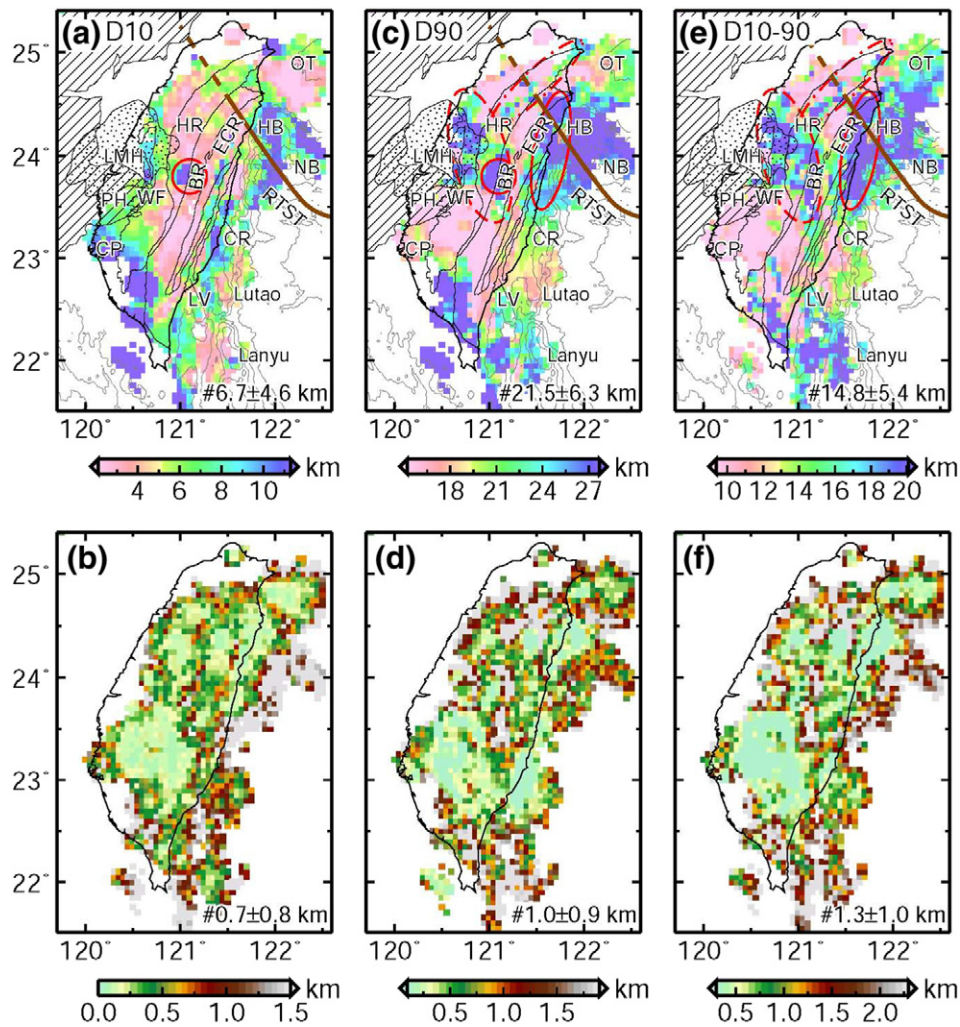


Fig. 4. Spatial variations of the seismogenic parameters (a, c and e) and their 1σ errors (b, d and f) for $D10$, $D90$ and $D10-90$, respectively. The numbers indicate the average values of 1σ errors. Symbol and layout are same to Fig. 1 except for: Brown lines define the western boundary of the Ryukyu-Taiwan stress transition (RTST); red circles in (a) and (c) mark a spot that has the deep onset and cutoff depths; in (c) and (e), red dashed lines delineate the NW-SE trending belt-like distributions of the deep cutoff depth and thick seismogenic thickness in central Taiwan; red dot-dashed lines outline a narrow zone with the deep cutoff depth and seismogenic thickness along the strike of the HR in northern Taiwan, and solid circles in northeastern Taiwan denote locations where have thick crust that has been revealed by tomographic images and receiver function analysis.

proposed an updip limit at 10 km depth for all subduction zones (Pacheco et al., 1993). More recently, Heuret et al. (2011) determined that the global average updip limit of the subduction seismogenic zones is 11 ± 4 km, which is close to our estimate (6.7 ± 4.6 km) of $D10$ within the 1σ uncertainty.

As illustrated in Fig. S1, the spatial distributions of the absolute values of SOD are different among $D1$, $D5$, and $D10$, but their relative spatial variations are robust. For instance, the SOD is remarkably deep in southwestern Taiwan and offshore eastern Taiwan. The regions with the intermediate onset depth are observed in the most parts of the Coastal Plain, the Western Foothills on the west, and the Coastal Range on the east. On other hand, the large-scale belt-like distribution with a NE-SW trend of the shallow SOD is clearly observed in central Taiwan, including most parts of the Hsuehshan Range, Backbone Range, and Eastern Central Range, which is roughly parallel to the strike of the geological structures of Taiwan. The SOD is also shallow in the Lutao-Lanyu region and in the southernmost part of the Okinawa Trough, where both these areas are known for hydrothermal activities.

Overall, the distribution pattern of the SOD in the island of the Taiwan is similar to the surface geological observations that the Taiwan mountain belt apparently separates rocks into discrete blocks of common age and grade by faults, and the age and metamorphic grade

generally increase from west to east (Ho, 1986). Meanwhile, the spatial variation of the SOD is similar to the observation in Japan that the seismicity onset depth is generally shallow in mountainous areas and particularly shallow in volcanic regions (Ito, 1999).

3.2. Spatial variation of the lower boundary of the seismogenic zone

The mean value of the SCD with the 1σ uncertainty is 21.4 ± 6.3 km for $D90$. By considering the 1σ uncertainty, the lower bound of the determined cutoff depth for $D90$ is 15.0 km, which is consistent with a typical value (15.0 km) of the seismicity cutoff depth for a vertical strike-slip fault (Shaw, 2013) and the average value (15.0 km) for south California (Nazareth and Hauksson, 2004). Wang et al. (1994) concluded that the depth of the peak in the earthquake number-focal depth relation is in the range of 4 to 8 km and suggested that 6 km is the mean depth of friction rupture and quasi-plastic deformation transition for the sub-regions in the island of Taiwan. In literature, the seismicity cutoff depth (i.e., seismic-aseismic transition) is interpreted either as the brittle-ductile transition (Sibson, 1986) or the unstable-stable sliding transition (Tse and Rice, 1986; Scholz, 1998) in the crust. It is reasonable to link the depth (6 km) of friction rupture and quasi-plastic deformation transition to the seismicity cutoff depth. However, the lower

bound of the SCD (15.0 km) is significantly larger than the mean transition depth (6 km) of the rheology between the frictional rupture and quasi-plastic deformation previously estimated by Wang et al. (1994). This discrepancy may be due to the fact that Wang et al. (1994) eliminated the relatively deep earthquakes in offshore and southwestern Taiwan, and particularly they used the depth of the peak in the seismicity rate to define the transition depth between the frictional rupture and quasi-plastic deformation. Because the seismicity we used was relocated by a high-resolution velocity model and the number of events is several times larger than that in previous studies, we propose that 15.0 km is a reasonable and conservative estimation for the seismic-aseismic transition in Taiwan on average.

The determined depth range for $D90$ (8.8–39.8 km) agrees well with that (5–40 km) determined by the 90% earthquake depth-frequency distribution in Japan (Omuralieva et al., 2012). However, unlike in Japan, where the variation trend of the SCD follows that of the SOD (Ito, 1999), in Taiwan, the spatial variation of the SCD is rather complicated. In detail, as shown in Fig. 4, the SCD remains rather deep in the offshore accretionary wedge off southwestern Taiwan and in the Hoping Basin offshore eastern Taiwan, which mimics the variation pattern of the SOD. The SCD is deep in mid-central Taiwan, where the SOD is shallow. Moreover, the belt-like distribution of the relatively deep SCD in central Taiwan (outlined by the dashed line in Fig. 4c) is mostly in a NW–SE trend and is sub-perpendicular to the strike of the major geological units of Taiwan. A narrow belt-like distribution of the deep SCD is observed in northern Taiwan (indicated by the dot-dashed line in Fig. 4c); its trend is parallel to the strike of the Hsuehshan Range. However, unlike the case of central Taiwan where a great number of grid nodes have deep SCDs, only a few grid nodes with relatively deep SCDs are observed in the limited portion of the Hsuehshan Range. These observations indicate that the correlation between the distribution of the SCD and the geological provinces is minor. This is probably because either the tectonostratigraphic provinces may not well represent the material properties at depths or the crustal composition may play a minor role in dominating the SCD.

In addition, a recent review of the rheology of the lithosphere studies proposed that the seismogenic layer thickness is 15–20 km on average (Burov, 2010), which is slightly less than the mean values (21–28 km) we determined for SCD ($D90$, $D95$, and $D99$). Note that the seismogenic layer thickness in the global compilation was determined by the focal depth distribution of intraplate earthquakes, which is different from ours, as we use earthquake depth-moment release accumulation.

3.3. Spatial variation of the seismogenic thickness

The ST beneath the Taiwan region is at a thickness of 3.8–33.6 km and the average thickness with the 1σ uncertainty is 14.8 ± 5.4 km for $D10$ – 90 . Fig. 4 exhibits that the first-order variation pattern of the ST is relatively thick in mid-central Taiwan, and offshore eastern and southeastern Taiwan. This pattern does not follow a general trend of the geological provinces of Taiwan and is more similar to the SCD rather than the SOD.

In Fig. 6, we observe that the ST is large under the central portion of Taiwan (indicated by the dashed line in Fig. 4e), which coincides with the presence of a thick crust > 50 km as revealed by tomographic images and receiver function analyses (e.g. Huang et al., 2014; Kuo-Chen et al., 2012a, 2012b; Wang et al., 2010a). Moreover, the ST is relatively large in the area between latitudes 23.5°N and 24.5°N and along the longitude 121.5°E (denoted by the dashed line in Fig. 4e), where the Moho depth is relatively deep. This region is located at the southernmost extent of the continental Moho under the southern Ryukyu Arc and the sub-vertical boundary between the Eurasia and Philippine Sea plates beneath the Taiwan orogeny (Lallemand et al., 2013). These observations suggest that the relatively large ST beneath mid-central and north-eastern Taiwan may relate to the collision between the Philippine Sea

and Eurasia plates and subduction of the Philippine Sea plate, respectively.

3.4. Anomalous deep seismogenic depths

It is worth mentioning that there exist two areas with anomalous deep earthquakes and, as a result, deep seismogenic depths. One is at the central part of Taiwan at 23.7°N and 121.0°E (indicated by a circle in Fig. 4). Many events with focal depths > 35 km exist in this area. These anomalous deep earthquakes have been observed, and using a mechanical model, have been attributed to the collocation of an eastward displacement of the Eurasian mantle at 24°N with a colder subducted crust of the south (Lin and Roecker, 1993). However, the proposed mechanical model neglects the effect of temperature on earthquake nucleation (Wang, 1998). By considering a present-day geothermal gradient of 30 °C/km in central Taiwan, as determined by Kuo-Chen et al. (2012a, 2012b), these earthquakes are considered to be deep (> 35 km); as a result, the temperature at focal depths may be higher than at the upper limit where continental earthquakes were thought to occur (~350 °C) (Devlin et al., 2012; McKenzie et al., 2005). Consequently, the causes of the intermediate-depth earthquakes beneath the central part of Taiwan and the deep seismogenic depths need further investigation.

The other area where anomalous deep earthquakes and deep seismogenic depths exist is the offshore accretionary wedge of southwestern Taiwan. Several early studies have indicated that earthquakes occurred commonly in the mantle of the oceanic lithosphere but rarely in continental mantle (e.g., Craig et al., 2014; Craig and Heyburn, 2015; Wiens and Stein, 1983). However, in the offshore accretionary wedge of southwestern Taiwan, which has the nature of the Eurasia continental lithosphere intrinsically, earthquakes frequently occurred mostly located within the upper mantle comprising the largely aseismic accretionary wedge. These anomalous mantle earthquakes have been attributed to the elevated pore pressure or the stress related to the bending and unbending of the subducted slabs (Cheng et al., 2012; Liao et al., 2008; Lin et al., 2009; Wu et al., 2009b).

4. Determination of the maximum magnitude for potential earthquakes

4.1. Procedure to determine the moment magnitude

Given the fault geometry of a seismogenic fault, we can determine the most likely moment magnitude (M_w) of a potential earthquake using the widely used empirical relations of the moment magnitude and rupture area (A) with respect to faulting types (Wells and Coppersmith, 1994):

$$M_w = 3.98 + 1.02 \log A, \text{ for strike-slip faults,}$$

$$M_w = 3.93 + 1.02 \log A, \text{ for normal faults, and,}$$

$$M_w = 4.33 + 0.90 \log A, \text{ for reverse faults.}$$

As is known, however, it is difficult to accurately determine the rupture area because a seismogenic fault may have a complex 3D structure. Such a difficulty leads us to use a simplified rectangular source model to calculate the rupture area of the known seismogenic fault. The rupture area A is defined as the product of the along-strike length (L) and the down-dip width (W) of a fault; that is, $A = L \times W$. To determine the rupture area, we directly adopt the fault length L , faulting types, and the average fault-dip angle δ of 20 major seismogenic faults from Shyu et al. (2005a) (Fig. 5 and Table 1), and the fault width is determined by our estimated ST.

Several approaches have been proposed to determine the fault width (See Fujiwara et al., 2009; Wells and Coppersmith, 1994). The most widely adopted approach is to use the depth distribution of after-shocks for visually determining the fault width (Wells and Coppersmith, 1994). However, this common way is highly subjective and often appears arbitrary. Meanwhile, previous studies have assumed

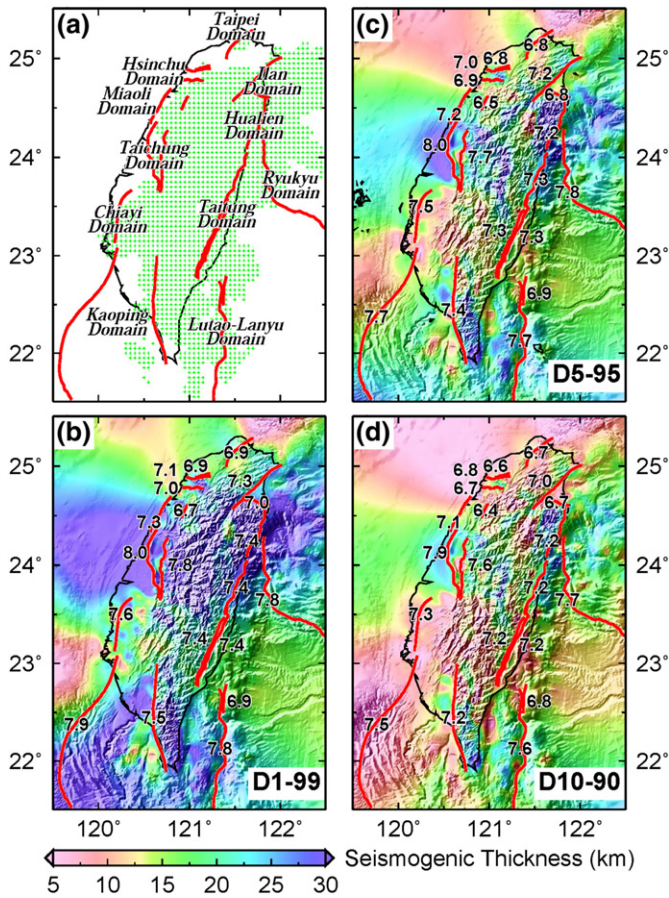


Fig. 5. (a) The locations of the major seismogenic faults (red lines) and the grid nodes (green crosses) used to determine the seismogenic depths. Numbers show moment magnitudes estimated by the optimal seismogenic thickness for D1–99 (b), D5–95 (c) and D10–90 (d).

that the rupture of the seismogenic fault extends to the surface, but the possibility that only a segment of the seismogenic fault ruptured to the surface could not be excluded. We also realize that current seismicity does not extend close to the surface, but this does not imply that the fault cannot break to the surface in the future. However, for most large earthquakes during past decades in Taiwan only very few ruptures extended to the surface. Therefore, for the short-term seismic hazard assessment, we prefer to use the ST (D1–99, D5–95, and D10–90) rather than the SCD (D90, D95, and D99) to approximate the fault width by taking the local upper boundary of the seismogenic zone as the top depth of the rupture extent.

For the computation of the moment magnitude in practice, we first extrapolate the ST over a 0.05°-resolution grid using the minimum curvature spline interpolator with a tension of 0.5 of the Generic Mapping Tools (Wessel and Smith, 1998) to cover some fault traces that are beyond the active seismogenic zone (Fig. 5). Then, the determined ST (H) and the average fault-dip angle (δ) from Shyu et al. (2005a) are used to derive the fault width W ($W = H/\sin\delta$). The inclusion of the along-strike variable fault-dip angle of the seismogenic fault would provide a more accurate constraint in the rupture area; however, such a dataset is not available for the Taiwan region at present. We thus use the average fault-dip angle instead. Finally, we determine the moment magnitude of a potential event through the empirical relation when the fault rupture area is obtained.

4.2. Limitations and uncertainties in determination of moment magnitude

Our approach cannot be applied to blind or buried faults whose existence was previously unknown. In our calculation, the mapped surface trace of the fault length is further allowed to be slightly discontinuous with small scale at the surface but can be considered as continuous at depth, as the active fault is not interrupted by a large-scale structural complexity. Meanwhile, many factors may inevitably be introduced into the determination of moment magnitude. For example, the fault traces may be incorrectly mapped on the surface, field data may be incorrectly digitized, and the fault-dip angle could be incorrectly assigned a value or faults could have a more complex shape.

Table 1

Fault parameters and our estimated moment magnitudes of potential events for 20 major seismogenic faults. NF is normal fault, RF is reverse fault and SS is strike-slip fault. Mw_O is the moment magnitude (M_w) determined by the optimum value of the seismogenic thickness for D1–99, D5–95 and D10–90. Mw_L and Mw_U are the lower and upper bounds of the moment magnitude that are determined by taking the 1σ uncertainty of the seismogenic thickness into account. The fault type and fault dip of the major faults (M_w _shyu) are adopted from Shyu et al. (2005a, 2005b). The moment magnitude estimated by Shyu et al. (2005a, 2005b) (M_w _shyu) is listed for a comparison.

Domain	Fault name	Fault type	Dip angle	Thickness & moment magnitude (M_w)									M_w _shyu
				D1–99			D5–95			D10–90			
				M_w _O	M_w _L	M_w _U	M_w _O	M_w _L	M_w _U	M_w _O	M_w _L	M_w _U	
Taipei Domain	Shanchiao fault, extend to Chinshan	NF	60	6.91	6.86	6.96	6.78	6.70	6.85	6.65	6.57	6.72	6.9
Hsinchu Domain	Northern fault on the Taoyuan-Hukou Tableland	RF	30	6.86	6.78	6.93	6.75	6.62	6.85	6.61	6.49	6.70	6.4
	Hukou fault	RF	30	7.09	7.02	7.15	6.99	6.86	7.08	6.84	6.71	6.94	6.9
Miaoli Domain	All Hsinchu-Hsincheng system	RF	45	6.95	6.91	6.99	6.85	6.77	6.91	6.71	6.61	6.79	6.8
	Shihtan fault	RF	75	6.68	6.62	6.72	6.53	6.48	6.57	6.44	6.41	6.47	6.1
Taichung Domain	Main detachment, only in Miaoli Domain	RF	30	7.2	7.6	7.7	7.1	7.2	7.8	7.09	6.99	7.7	7.3
	Chelungpu fault	RF	15	7.82	7.78	7.86	7.69	7.65	7.73	7.59	7.55	7.63	7.6
Chiayi Domain	Changhua fault	RF	10	8.04	8.00	8.08	7.95	7.89	8.00	7.85	7.79	7.90	7.7
	Main detachment	RF	15	7.64	7.57	7.70	7.46	7.37	7.53	7.33	7.26	7.39	7.5
Kaoping Domain	Deformation front	RF	30	7.86	7.78	7.94	7.69	7.50	7.82	7.50	7.29	7.63	>7.7
	Chaochu fault connecting the offshore fault	RF	75	7.48	7.44	7.52	7.35	7.29	7.39	7.23	7.18	7.28	7.3
Illan Domain	Northern Illan fault system	NF	60	7.33	7.30	7.36	7.20	7.14	7.25	7.04	6.98	7.1	7.2
	Southern Illan fault system	NF	60	7.01	6.99	7.02	6.84	6.81	6.86	6.65	6.62	6.68	6.6
Ryukyu Domain	Major right-lateral accommodation structure	SS	90	7.36	7.35	7.37	7.24	7.23	7.24	7.15	7.14	7.16	6.9
	Ryukyu trench	RF	30	7.78	7.75	7.80	7.71	7.67	7.75	7.64	7.59	7.68	8.0
Hualien Domain	Longitudinal fault, Hualien Domain only	SS	60	7.38	7.37	7.39	7.31	7.30	7.32	7.22	7.20	7.23	7.2
Taitung Domain	Central Range fault, total	RF	45	7.37	7.36	7.38	7.29	7.27	7.31	7.19	7.17	7.22	7.2
	Longitudinal fault, Taitung Domain only	RF	60	7.37	7.35	7.38	7.29	7.26	7.31	7.20	7.17	7.2	7.2
Lutao-Lanyu Domain	Huatung Ridge fault	RF	30	7.82	7.80	7.83	7.77	7.73	7.80	7.70	7.65	7.73	7.6
	West Lutao fault	RF	45	6.93	6.90	6.95	6.86	6.82	6.89	6.80	6.76	6.83	7.0

It is widely accepted that the width of the rupture area is limited by the finite thickness of the seismogenic zone. Nevertheless, theoretical studies have shown that coseismic slip may extend below the base of the seismogenic zone (Hillers and Wesnousky, 2008; Shaw, 2013; Shaw and Wesnousky, 2008). On the other hand, Rolandone et al. (2004) and Taira et al. (2008) have used temporal changes in depth distribution of aftershocks to reveal a deepening SCD following the 1992 $M7.3$ Landers earthquake and the 2004 $M6$ Parkfield earthquake. Under the premise that the above-mentioned coseismic SCD deepening commonly occurs for large earthquakes, the fault width determined by spatial distributions of the coseismic slip or aftershocks would be larger than those determined by our estimated ST. Note that the fault widths determined by different datasets or methods have different physical meanings. For example, the fault width determined using the coseismic slip model may present the source area with the coseismic moment release (Lay and Kanamori, 1980; Yamanaka and Kikuchi, 2004; Yen and Ma, 2011). Many researchers have reported that aftershocks occur mostly in the regions of low coseismic slip where shear stress is increased (Woessner et al., 2006), and thus, the fault width derived from aftershock distribution can be viewed as the area with high shear stress. The determination of the fault width in our method is based on the background earthquake depth-moment release distribution, and the determined fault area can be considered as the area where the interseismic elastic strain has been accumulated in the crust.

There are some uncertainties in the precise relationship between the ST and fault width and possible ambiguity of deep coseismic slip below the seismogenic zone (Shaw, 2013). To accommodate the coseismic deepening of aftershocks for large earthquakes, Shaw (2013) proposed to convert the cutoff depth (D) to the fault width by multiplying a constant parameter ξ ($W = \xi D / \sin \delta$), where $\xi \geq 1$. However, due to lack of knowledge on determination of the parameter ξ , we do not consider the influence of coseismic deepening of aftershocks and our determined moment magnitude could be considered a conservative estimation.

The method we used to determine the rupture extent and moment magnitudes of potential earthquakes is limited in terms of the number of assumptions, particularly that the seismogenic zone is determined by the distribution of seismicity, and the time span of our seismicity catalog is much shorter than the recurrence intervals of large earthquakes. Whether the short seismic record can be used to represent the long-term seismic behavior of a fault is debatable. Thus, our intention is not to demonstrate the robustness of our method in determining magnitudes of potential large earthquakes, but to provide an alternative database for scenario earthquake simulation and evaluate strong motions for seismic hazard assessment. This is particularly critical for areas that are not studied sufficiently and related data are either sparse or unavailable. Moreover, tsunami earthquakes are considered a special class of earthquakes that almost exclusively rupture to the surface; these are not our focus at present.

5. Earthquake potential of the major seismogenic faults

The maximum magnitude of a potential earthquake estimated by $D1-99$, $D5-95$, and $D10-90$ ranges from $Mw6.4$ to 8.0 (Fig. 5 and Table 1). For a given seismogenic fault, the difference in determined moment magnitudes by $D1-99$, $D5-95$, and $D10-90$ is generally within 0.3 , which completely reflects the influence of the estimated ST. It is noticeable that the determined magnitude of the Chelungpu fault for a potential rupture estimated by $D10-90$ is $Mw7.6$, which is consistent with the moment magnitude of the Chi-Chi earthquake that is determined by the global centroid-moment tensor inversion (Dziewonski et al., 1981). We appreciate that the Chi-Chi earthquake aftershocks may dominate the determination of the seismogenic depths in central and western Taiwan. The depth ranges and mean values (in parenthesis) of the local upper ($D10$) and lower ($D90$) boundaries of the seismogenic zone along the Chelungpu fault trace are $5.6-11.1$ km (8.1 km) and $15.8-27.7$ km (22.8 km), respectively. This result is inconsistent with the

observation that the Chi-Chi earthquake rupture of the Chelungpu fault extends from a depth of approximately 15 km to the ground surface (Kao and Chen, 2000). However, our determined ST ($D10-90$) along the Chelungpu fault trace ranges $7.0-20.7$ km and its mean value is 14.7 km, in accordance with the depth distribution (~ 15 km) of the Chi-Chi earthquake main rupture and aftershocks (Chang et al., 2007; Kao and Chen, 2000). In other words, the average ST along the Chelungpu fault trace is comparable to the rupture depth extent of the Chi-Chi earthquake. If $D90$ ($16.8-24.0$ km) along the Chelungpu fault is used to present the fault width, the moment magnitude of the Chi-Chi earthquake would be overestimated. Thus, the ST ($D10-90$) seems to be a more reasonable approximation of the fault width than the SCD ($D90$). We understand that more case studies are necessary to validate our approach, but the Chi-Chi earthquake is the only event well-studied using seismic data recorded by modern digital seismographs in the past decades. In the following sections, we will show that our estimated magnitudes of most large earthquakes are consistent with results of previous studies. This leads us to believe that our method is reasonable in determining the moment magnitude of a potential earthquake. Moreover, the moment magnitude estimated by $D10-90$ could be viewed as a conservative estimation.

5.1. Western Taiwan

In our calculation, the largest earthquake ($Mw7.9-8.0$) may occur in western Taiwan along the Changhua fault (Fig. 5 and Table 1). The magnitude determined by our method is in good agreement with the estimates in previous studies (e.g. Cheng et al., 2007; Shyu et al., 2005a); however, it is significantly larger than the magnitude ($M7.1$) of the February 12, 1848 earthquake, which may relate to the Changhua fault (Tsai, 1985).

An earlier study of the time-dependent probabilistic seismic hazard analysis (PSHA) suggested that the occurrence of the 1999 Chi-Chi earthquake may increase the potential of seismic hazard caused by the Changhua fault rupture (Lee, 2004). Furthermore, Mouyen et al. (2010) showed a significant Coulomb stress increase in the southern part of the Changhua fault by taking into account the interseismic deformation and coseismic stress change caused by major earthquakes over the past three centuries. Note that the recurrence interval of the Changhua fault was estimated in the range between 153 and 226 years (Lee, 2004). After a quiescence of about 169 years for the Changhua fault, along with the above-mentioned studies, we propose that the seismic hazard potential in western Taiwan is relatively high and seismic hazard mitigation should be a matter of urgent concern.

Under the Taiwan tectonic framework, blind faults are expected to widely distribute in western Taiwan (Wu and Rau, 1998). However, due to the unknown fault geometry of blind faults, we cannot determine the most likely moment magnitudes for blind faults by our approach. Regarding the highly risky potential caused by blind faults, geophysical surveys and drillings should be conducted for blind fault recognition for the Taiwan region, particularly in the western part of Taiwan.

Moreover, as mentioned in Section 1, the PH and LMH may be linked to the occurrence of earthquakes and the spatial variation of the tectonic stress in western Taiwan. We thus examine if the PH and LMH are correlated with the spatial distribution of seismogenic depths. As shown in Fig. 4, only the limited portions of the PH and LMH have the resolution of the seismogenic depths. In both the PH and LMH, the SOD is mostly intermediate and few sub-areas have a relatively deep SOD. In other words, there is no difference in the variation patterns of the SOD between the PH and the LMH. On the other hand, the SCD in the LMH is deeper than that in the PH, and the relatively deep SCD is located on the northeastern corner of the LMH. The variation pattern of the ST in the PH and LMH is similar to that of the SCD (Fig. 4). These observations indicate that the LMH is capable of generating earthquakes at relatively deep depths. Therefore, the inclusion of blind faults and the LMH in

scenario earthquake simulations would lead us to better establishing the more complete and reliable seismic hazard models.

5.2. Taipei metropolitan area

The Taipei Metropolitan Area is the political, economic, and cultural center of Taiwan. Much attention should be paid to seismic hazard evaluation in this area (Kanamori et al., 2012; Wang et al., 2010b; Wang, 2008; Wang et al., 2011). Two faults, the Chinshan and Shanchiao faults, may relate to the M7 earthquake that occurred in the Taipei region in 1694 (Wang et al., 2010b). On the basis of the numerical modeling result, Wang et al. (2010b) proposed that the rupture of the Shanchiao fault most likely triggers the Chinshan fault to fail. Accordingly, a conservative seismic hazard assessment for the Taipei Metropolitan Area is to assume the Chinshan and Shanchiao faults rupture simultaneously. Under this scenario, the maximum magnitude of a potential earthquake that occurs in the Shanchiao and Chinshan fault system is $M_w6.7$ – 6.9 (Fig. 5 and Table 1), which is consistent with the magnitude ($M_w6.9$) determined by Shyu et al. (2005a) and Cheng (2002). On the other hand, Huang et al. (2007) used stratigraphic data of boreholes to argue that the maximum-size earthquake might mainly occur along the Shanchiao fault and the moment magnitude would be in the range $M6.9$ – 7.1 . Obviously, Huang et al. (2007) provided a different scenario for the seismic hazard assessment in the Taipei Metropolitan Area. Our intent is not to resolve whether the Chinshan fault will rupture but to demonstrate that the Taipei basin is capable of generating a large earthquake ($M \geq 6$). Our estimated moment magnitude ($M_w6.7$) for the Shanchiao and Chinshan fault system can be considered as a conservative estimation and could be a basis for a future integral scenario study by taking into account factors such as basin amplification, topography, earthquake location, and fault orientation (e.g., Lee et al., 2008a; Lee et al., 2008b; Miksat et al., 2008).

5.3. Southernmost Ryukyu subduction zone

In addition to the earthquakes that occurred in the Taipei area, eastern offshore earthquakes such as the Hualien offshore earthquakes of May 20 and November 14, 1986 (Chen and Wang, 1988) and March 31, 2002 (Chen, 2003) (Fig. 1) caused serious damage to Taipei city. Therefore, the evaluation of the seismic potential in the southern Ryukyu subduction zone is also a crucial issue (Hsu et al., 2013; Hsu et al., 2012; Kao, 1998).

Earthquakes at the southernmost Ryukyu zone occur on the accretionary prism, interplate interface, and splay faults (Theunissen et al., 2012). To exclusively separate the effects of different fault systems on the occurrence of earthquakes is difficult. We thus follow Shyu et al. (2005a) and take the subduction interface as the predominate structure in this area for the seismic hazard assessment.

Kao (1998) used the interplate earthquakes to illustrate that the updip and downdip limits of the interplate seismogenic zone in the southernmost Ryukyu subduction zone locate at 10 km and 35 km, respectively. Based on the geometric configuration of the subducted slab interface, Kao (1998) further determined that the most likely magnitude of a future event in the southernmost Ryukyu subduction zone is $M_w7.6$ – 7.7 , which is close to our estimation ($M_w7.7$ – 7.8) (Fig. 5 and Table 1) but slightly smaller than that ($M_w8.0$) of Shyu et al. (2005a). Furthermore, Hsu et al. (2012) inverted the interseismic GPS data along the Hualien-Taitung coast and proposed that an $M_w7.5$ – 8.7 earthquake may occur in this region.

Wu et al. (2010) used the orientation of the compressional stress axis to identify a triangular area between the southernmost Ryukyu subduction zone and Taiwan, which is referred as the Ryukyu–Taiwan Stress Transition (RTST). The western boundary of the RTST coincides with the border that separates the post-collision and waning-collision domains in northern Taiwan; it is particularly close to the surface traces of the tear fault proposed by previous studies (Wu et al., 2010). We

expect that the RTST may alter the seismogenic depths. However, no significant correlations between the western boundary of the RTST and the seismogenic parameters are observed (Fig. 4). Thus, the RTST generally have minor influence in the seismogenic depths.

5.4. Offshore southwestern Taiwan

Offshore southwestern Taiwan (21.5°N – 23°N), the incipient arc-continent collision zone between the Luzon volcanic arc and the Eurasia Plate, is considered a region with high seismic and tsunami risk (Lin et al., 2009). However, in this region, the geometry of the subduction seismogenic zone cannot be well revealed by either earthquake focal mechanisms (e.g., Kao et al., 2000) or seismic reflection studies (e.g., Eakin et al., 2014; Lester et al., 2014; Lester et al., 2013; McIntosh et al., 2005) for seismic hazard assessment. Fortunately, our proposed method provides an alternative to determine seismogenic depths and to evaluate seismic potential. The estimated magnitude of a future event along the deformation front in the offshore southwestern Taiwan is $M_w7.5$ – 7.9 , which is consistent with the lower bound ($M > 7.7$) of the estimation by Shyu et al. (2005a, 2005b) (Fig. 5 and Table 1).

In addition, on the basis of the maximum-likelihood Gutenberg–Richter relation with an assumption of Gaussian probability distribution, Chen et al. (2008) suggested that the probability of an $M7.0$ earthquake to occur in this area within the next 50 years is 20% after the December 26, 2006 Pingtung doublet earthquakes. This result implies that the seismic risk is low at present or in the immediate future. However, in this area large anticlinal ridges and thrust faults have been observed (Shyu et al., 2005a; Shyu et al., 2005b). Furthermore, a number of splay faults exist in the upper-slope wedge (Lin et al., 2009; Lin et al., 2013; Zhu et al., 2013) and a series of blind thrusts is developing in the lower-slope wedge (Lin et al., 2008). The stability and extension of the splay faults and developing blind thrusts are one of the major concerns for the occurrence of potential large earthquakes (e.g. Hsu et al., 2013) and should be investigated in detail for seismic hazard mitigation.

5.5. Longitudinal Valley

The PSHA study indicated that apart from the Western Foothills, the Longitudinal Valley is a region with high seismic risk (Cheng et al., 2007). Our results show that the rupture by the Longitudinal Valley fault in either the Hualien region or the Taitung region, or the total Central Range fault may produce a $M_w7.2$ – 7.4 event (Fig. 5 and Table 1), which is slightly larger than the magnitude ($M_w7.2$) estimated by Shyu et al. (2005a).

Geodetic evidence and geologic observations have shown that the Longitudinal Valley fault is creeping in south and locked in north (e.g. Angelier et al., 1997; Lee et al., 2003; Lee et al., 2001; Yu and Kuo, 2001; Yu and Liu, 1989). A recent numerical modeling based on geodetic and geologic data further revealed that the southern segment of the Longitudinal Valley fault is creeping at a rate of 5–28 mm/yr down to a depth of 15–20 km, while the northern segment is locked from the surface to a depth of 20 km (Huang et al., 2010). It has been intuitively expected that the creeping section of the Longitudinal Valley fault has low potential for large earthquakes based on the assumption that the large portion of the accumulated seismic strain has been released aseismically. This assumption seems to be validated through the observation that no large earthquakes and obvious surface rupture have been observed along the southernmost part of the Longitudinal Valley fault (Chuang et al., 2012). On the other hand, the locked segment of the Longitudinal Valley fault has been assumed to be increasing earthquake risk because compressional stress is enhancing.

A more recent numerical simulation of earthquake nucleation proposed that the creeping segment of the faults may rupture under appropriate conditions (Noda and Lapusta, 2013). Furthermore, the creeping section of the Longitudinal Valley fault is able to generate coseismic rupture, which is supported by the spatial distributions of moderate

earthquakes and the associated aftershocks as well as the coseismic slip (e.g., Ching et al., 2007; Hu et al., 2007; Kuo-Chen et al., 2004; Kuo-Chen et al., 2007; Thomas et al., 2014; Wu et al., 2006a; Wu et al., 2006b). Consequently, the possibility that a large earthquake occurs in the southern segment of the Longitudinal Valley fault cannot be ruled out.

At present, it remains unknown how fault slip behaviors affect the occurrence of earthquakes, which complicates the determination of the most likely moment magnitude of a potential earthquake that occurs in this region on the basis of the background seismicity alone. Accordingly, the seismic hazard assessment in the Longitudinal Valley fault is a delicate issue and shall be examined in detail in the future.

In addition, Smith-Konter et al. (2011) showed that the fault locking depth derived from geodetic models agrees with the SCD, although the geodetic locking depth represents the effective thickness of the fault zone of the interseismic strain accumulation, but the SCD illustrates a transition depth from the seismic faulting to aseismic slip. A comparison between the SCD determined by us and the fault locking depth estimated by Huang et al. (2010) along the Longitudinal Valley fault shows that the SCD is generally deeper than the geodetic locking depth within 5–10 km. In detail, the southern segment of the Longitudinal Valley fault is creeping at a rate of 5–28 mm/yr down to a depth of 15–20 km, where the SCD is in the range 17–24 km with a mean value of 19 km, while the northern segment is locked from the surface to a depth of 20 km, where the SCD is in the range 21–27 km with a mean value of 23 km. It is difficult to determine whether the SCD or the geodetic locking depth is more appropriate for seismic hazard assessment. Thus, both geodetic locking depth and SCD shall be considered in the earthquake hazard model to provide simulation of different scenario earthquakes.

6. Relation between seismogenic parameters and earthquake source parameters

6.1. Dependence of seismogenic parameters on earthquake faulting types

On the basis of a conventional multi-layer continental crust rheology model, the transition depth of the brittle to ductile deformation (i.e., the SCD) for different fault types would be the deepest for normal faulting, shallowest for thrusting faulting, and intermediate for strike-slip faulting (Sibson, 1974; Sibson, 1982; Sibson, 1984). Because under the same conditions, the thrust fault must act against gravity and requires larger shear stress to overcome fault strength (Doglioni et al., 2011),

the SCD for thrust faulting events is shallowest. Moreover, Wang et al. (1994) concluded that seismicity depth in Taiwan is dominated by the earthquake faulting types. Taking advantage of the abundant first-motion focal mechanism solutions (e.g. Wu et al., 2008), we perform a more general analysis by examining the relation between the earthquake faulting types and the seismogenic depths in detail.

To this end, we categorize shallow events (depth ≤ 50 km) with first-motion focal mechanisms between 1990 and 2015 based on the plunge of the tensional axis (pt) and plunge of the null axis (pb), as described by Triep and Sykes (1997) and Reasenber (1999): thrust (pt > 45), normal (pt < 45 and pb < 45), and strike-slip (pb > 45). To further reduce the effect of the uncertainty of focal mechanism solutions on statistical results, only the high-quality events, i.e., a quality value > 1 (Wu et al., 2008), are used. In total, 3249 events with $M_w \geq 1$ are used in this study. Among them, 1338 (41%) events are thrust-faulting type, 725 (22%) events are normal-faulting type, and 1186 (37%) events are strike-slip faulting-type (Fig. 6).

By using 2000 bootstrap resamples, we determine the mean value and the 1σ uncertainty of the seismogenic parameters for all the selected events with or without considering the faulting types. Fig. 7 shows that the seismogenic parameters are dependent on faulting types. In detail, within the 1σ uncertainty, the SOD is shallowest for normal faulting events, deepest for thrust events, and intermediate for strike-slip events for D_{10} . On the other hand, the SCD is the shallowest for strike-slip events, deepest for thrust events, and intermediate for normal faulting events for D_{90} . The variation pattern of the ST (D_{10} – 90) generally follows that of the SCD. These results are also confirmed by other depth ranges of the seismogenic parameters (Fig. S6). The dependence of the SCD on faulting types is different from the prediction of the conventional rheology model (Sibson, 1974; Sibson, 1982; Sibson, 1984). This discrepancy can be attributed to the fact that our observations include the lateral variations related to the seismogenic characteristics of oceanic (Philippine Sea Plate) and continental (Eurasia Plate) lithospheres, whereas the conventional rheology model is based on the assumption of the continental crust composition. Therefore, to explain our observation in detail, a more sophisticated crustal rheology model must be re-parameterized with geological temporal and spatial scales for Taiwan.

Our results demonstrate that the SCD is the shallowest for strike-slip events, intermediate for normal events and deepest for thrust events. This pattern is consistent with the conclusion from many global and regional studies that strike-slip earthquakes have higher stress drop and apparent stress than normal and thrust earthquakes (e.g. Allmann and

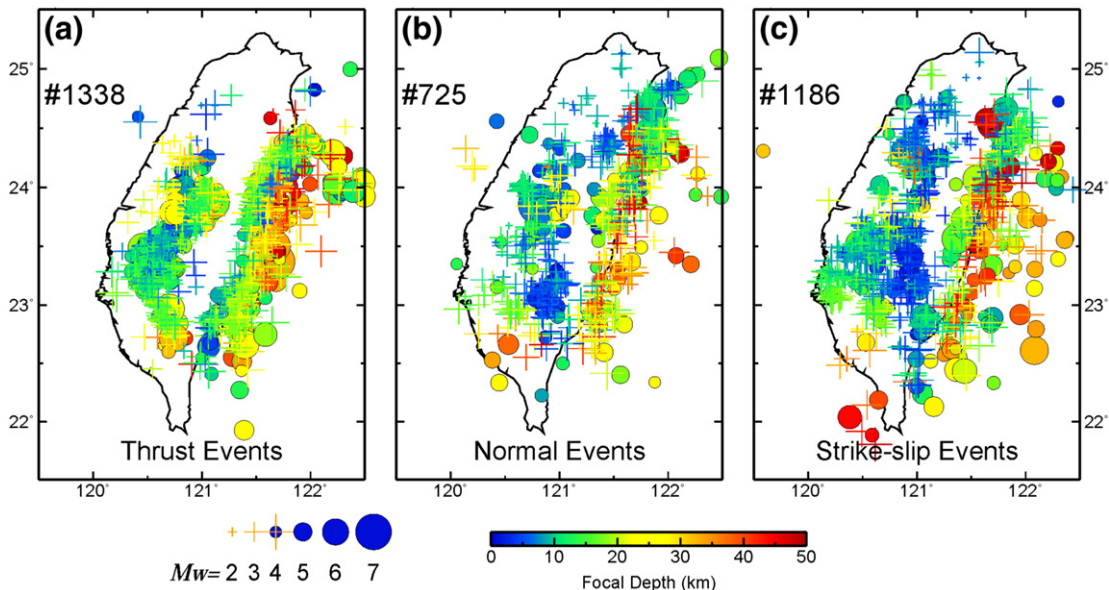


Fig. 6. Distribution of shallow (depth ≤ 50 km) earthquakes with different fault types. (a) thrust; (b) normal (c) and strike-slip.

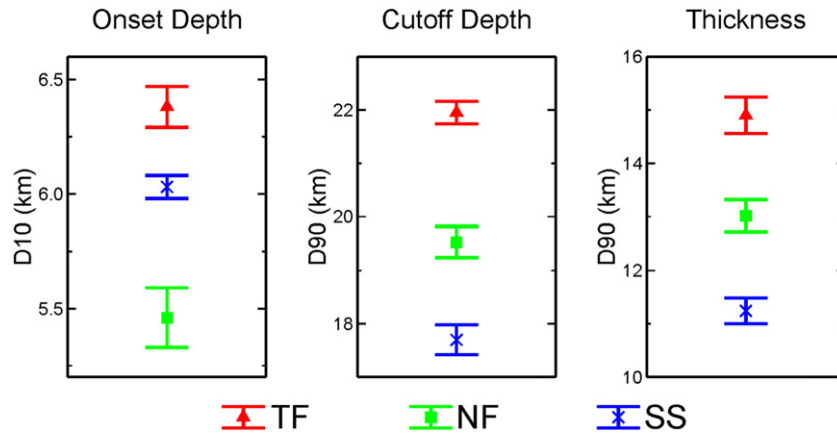


Fig. 7. The mean values of the seismogenic parameters with respect to faulting types including, thrust (TF), normal (NF) and strike-slip (SS) shallow (≤ 50 km) earthquakes. The means and 1σ uncertainties are shown in different symbols and bars, respectively.

Shearer, 2007, 2009; Choy and Boatwright, 1995; Prieto et al., 2004; Wu et al., 2013); however, there is no widely accepted explanation for these observations at present (Allmann and Shearer, 2009). To find an appropriate model to interpret the dependences of the seismogenic parameters on the earthquake faulting types is beyond the scope of this study.

6.2. Relation between moderate–large earthquake focal depth and seismogenic depth

The determination of the moment magnitude using the ST in this study implicitly assumes that the rupture can initiate at any depth within the seismogenic zone and extend through the whole seismogenic zone. However, many previous studies have argued that moderate to large earthquakes tend to occur near the bottom of the seismogenic zone (e.g., Das and Scholz, 1983; Ito, 1990; Sibson, 1982; Sibson, 1984; Yang et al., 2012). To understand if the above-mentioned observation also exists for Taiwan, we first retrieve moderate to large ($M_w \geq 4$) events from the first-motion focal mechanism catalog compiled in Section 6.1. In total, there are 762 events with moment magnitude (M_w) ranging from 4.0 to 7.6. Among them, there are 395 (52%) events with thrust faulting, 140 (18%) events with normal faulting, and 227 (30%) events with strike-slip faulting. Fig. 6 shows that the selected events are widely distributed around the seismogenic areas of Taiwan rather than in a specific area. Therefore, these events well sample the common characteristics of the focal depth and seismogenic depth for the seismogenic structures in Taiwan. We then determine the linear cross-correlation coefficients (Pearson's coefficient, R) between the focal depth and the seismogenic depth for all the events (Press et al., 1992), and use 1000 bootstrap resamples to estimate the mean value and 1σ uncertainty. Here the seismogenic depth is determined by using the value of the maximum percentage of the earthquake depth–moment distribution from 5% to 95% with an increase of 5% (1% and 99% are also included). We define that the top portion of the seismogenic zone is the area of $D1$ – $D35$, the middle portion is $D35$ – $D70$, and the bottom portion is $D70$ – $D99$. The finite source dimension of large earthquakes and the possibility of coseismic-slip penetrating below the bottom of the seismogenic zone (e.g. Hillers and Wesnousky, 2008; Shaw, 2013; Shaw and Wesnousky, 2008) are neglected because we are interested in the relation between the earthquake nucleation depth and the seismogenic depth.

Fig. 8a shows that regardless of the faulting types, the focal depth has the strongest correlation coefficient of R with the seismogenic depth of $D80$, and it is statistically associated with the seismogenic depth from $D75$ to $D90$ within 1σ uncertainty. In this case, it seems be reasonable to suggest that intermediate to large crustal earthquakes may tend to occur at the bottom portion of the seismogenic zone. By further taking the faulting types into account, the focal depth has the strongest

correlation with $D80$ for strike-slip events, $D85$ for thrust events, and $D65$ for normal events (Fig. 8b, c, and d). Within the 1σ uncertainty, the focal depth is significantly correlated with the seismogenic depth from $D75$ to $D90$ for thrust events and from $D50$ to $D90$ for strike-slip, and from $D35$ to $D85$ for normal events. Hence, no statistical evidence is obtained to support that the relation between the seismogenic depth and focal depth is dependent on the faulting types. Furthermore, strike-slip and normal events may occur at the middle to bottom of the seismogenic zone. We also repeat the above-mentioned procedures to determine the relations between the focal depth and seismogenic depth for larger events ($M_w \geq 5$) and obtain slightly different results, but with large uncertainty bounds.

7. Conclusions

We have illustrated the spatial distribution of the seismogenic parameters for the whole of Taiwan in unprecedented resolution. In general, the spatial distribution of seismicity in the Taiwan region can be explained largely by the convergence between the Eurasia and Philippine Sea plates, but the seismogenic depths reveal a more complex pattern. For the first-order variation pattern, the relative shallow SOD follows the general structural trend of the Taiwan mountain belt, and the SCD is relatively deep in the central portion of Taiwan.

Our results provide the potential updip and downdip limits for the earthquake rupture and the estimation of moment magnitudes for seismogenic faults. The largest potential earthquake would be produced by the Changhua fault in western Taiwan. The blind-thrust faults could cause serious damage and are expected to distribute in much of western Taiwan. Therefore, a more detailed blind fault recognition using geophysical surveys and drilling are urgently needed to make effective mitigation plans for seismic hazard in western Taiwan.

We have found that for crustal earthquakes, normal events have the shallowest SOD, but strike-slip events have the shallowest SCD. Such a dependence of the seismogenic depths on faulting types cannot be interpreted by the traditional continental rheology model and needs to be studied in detail in future. We also have observed that for intermediate to large crustal earthquakes the relations between the focal depth and the seismogenic depth have no statistical correlation with the faulting types. Regardless of the faulting types, earthquakes tend to occur at the bottom portion of the seismogenic zone, which is consistent with previous observations in California and Japan. With respect to the faulting types, thrust events tend to occur at the bottom portion of the seismogenic zone, but strike-slip and normal events are distributed at a large depth range of the seismogenic zone.

In addition to determining the maximum moment magnitudes of potential earthquakes, the spatial distribution of the seismogenic depths (i.e., the upper and lower boundaries of the seismogenic zone)

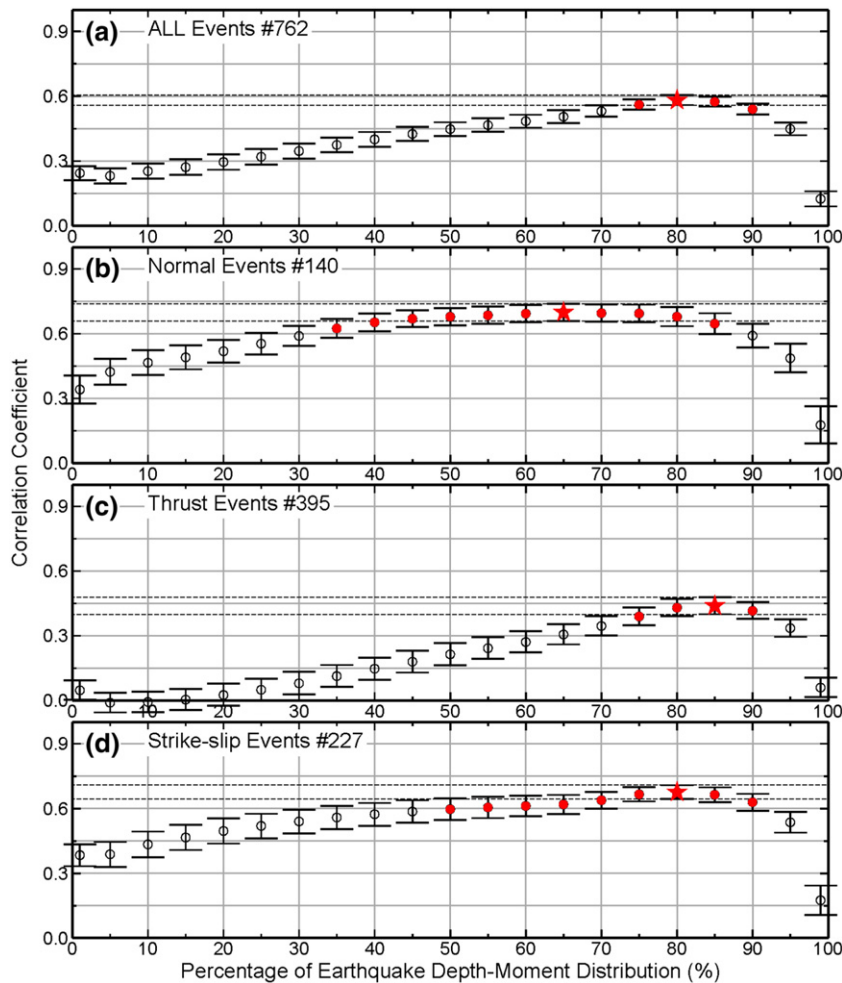


Fig. 8. The correlations between the seismogenic depths and the earthquake focal depths of shallow (≤ 50 km; $\geq M_w 4.0$) earthquakes with and without taking into account faulting types. The means and 1σ uncertainties are shown in circles and bars, respectively. The star marks the mostly correlated relation between the seismogenic depth and the focal depth, and the relations within 1σ uncertainties are presented by solid circles.

can be used to examine the effect of the non-planar geometry for blind faults on strong ground motion. Moreover, our results can further pose a constraint on the determination of the locking depth of a fault, which is required to model the deformation on the fault system. Since our findings are helpful to improve seismic hazard models, our approach is worth applying to other regions. However, our approach relies heavily on the quality and quantity of the earthquake catalog; in fact, the Southern California and Japan would be the best candidates for application and calibration of our approach.

Finally, note that the factors that govern the spatial distribution of seismogenic depths in Taiwan remain controversial. Therefore, our future step is to examine the relations between seismogenic depth and a variety of available geophysical observations.

Acknowledgements

We are grateful to the editor Kelin Wang and two anonymous reviewers for their constructive comments and suggestions. We thank the Central Weather Bureau for providing the earthquake data. During the development of the manuscript, we benefited from useful and spirited conversations with Wen-Bin Doo, Hsin-Hua Huang, Yin-Sheng Huang, Chung-Ling Lo, Yang Li, J. Bruce H. Shyu, and Louis S. Teng. The first author was financially supported by Institute of Earth Sciences, Academia Sinica, Center for Environmental Studies of National Central University, and Ministry of Science and Technology of Taiwan, Republic of China, under grants NSC-102-2811-M-001-020, NSC-103-2811-M-

001-025, and MOST-104-2811-M-001-053. All figures were prepared using the Generic Mapping Tools (Wessel and Smith, 1998).

Appendix A. Supplementary data

Supplementary data to this article can be found online at <http://dx.doi.org/10.1016/j.tecto.2017.04.028>.

References

- Allmann, B.P., Shearer, P.M., 2007. Spatial and temporal stress drop variations in small earthquakes near Parkfield, California. *J. Geophys. Res.* 112, B04305.
- Allmann, B.P., Shearer, P.M., 2009. Global variations of stress drop for moderate to large earthquakes. *J. Geophys. Res.* 114, B01310.
- Angelier, J., Chu, H.T., Lee, J.-C., 1997. Shear concentration in a collision zone: kinematics of the Cihshang fault as revealed by outcropscale quantification of active faulting, Longitudinal Valley, eastern Taiwan. *Tectonophysics* 274, 117–143.
- Bonner, J.L., Blackwell, D.D., Herrin, E.T., 2003. Thermal constraints on earthquake depths in California. *Bull. Seismol. Soc. Am.* 93, 2333–2354.
- Burov, E.B., 2010. The equivalent elastic thickness (T_e), seismicity and the long-term rheology of continental lithosphere: time to burn-out “crème brûlée”? insights from large-scale geodynamic modeling. *Tectonophysics* 484, 4–26.
- Chang, C.-H., Wu, Y.-M., Zhao, L., Wu, F.T., 2007. Afterhock of the 1999 Chi-Chi, Taiwan, earthquake: the first hour. *Bull. Seismol. Soc. Am.* 97, 1245–1258.
- Chen, K.C., 2003. Strong ground motion and damage in the Taipei basin from the Moho reflected seismic waves during the March 31, 2002, Hualien, Taiwan earthquake. *Geophys. Res. Lett.* 30, 1551.
- Chen, K.-C., Huang, W.-G., Wang, J.-H., 2007. Relationships among magnitudes and seismic moment of earthquakes in the Taiwan region. *Terr. Atmos. Ocean. Sci.* 18, 951–973.

- Chen, K.-C., Wang, J.-H., 1988. A study on aftershocks and focal mechanisms of two 1986 earthquakes in Hualien, Taiwan. *Proc. Geol. Soc. China* 65–72.
- Chen, P.-F., Newman, A.V., Wu, T.-R., Lin, C.-C., 2008. Earthquake probabilities and energy characteristics of seismicity offshore Southwest Taiwan. *Terr. Atmos. Ocean. Sci.* 19, 697–703.
- Chen, W.-P., Hung, S.-H., Tseng, T.-L., Brudzinski, M., Yang, Z., Nowack, R.L., 2012. Rheology of the continental lithosphere: progress and new perspectives. *Gondwana Res.* 21, 4–18.
- Chen, W.P., Molnar, P., 1977. Seismic moments of major earthquakes and the average rate of slip in central Asia. *J. Geophys. Res.* 82, 2945–2969.
- Chen, Y., Shin, T., 1998. Study on the earthquake location of 3-D velocity structure in the Taiwan area. *Meteor. Bull.* 42, 135–169.
- Cheng, C.-T., 2002. Uncertainty Analysis and Deaggregation of Seismic Hazards. Institute of Geophysics, National Central University, Chung-Li, Taiwan, p. 197.
- Cheng, C.-T., Chiou, S.-J., Lee, C.-T., Tsai, Y.-B., 2007. Study on probabilistic seismic hazard maps of Taiwan after Chi-Chi earthquake. *J. Geol.* 2, 19–28.
- Cheng, C.-T., Lee, C.-T., Lin, P.-S., Lin, B.-S., Tsai, Y.-B., Chiou, S.-J., 2010. Probabilistic earthquake hazard in Metropolitan Taipei and its surrounding regions. *Terr. Atmos. Ocean. Sci.* 21, 429–446.
- Cheng, W.-B., Hsu, S.-K., Chang, C.-H., 2012. Tomography of the southern Taiwan subduction zone and possible emplacement of crustal rocks into the forearc mantle. *Glob. Planet. Chang.* 90–91, 20–28.
- Ching, K.-E., Rau, R.-J., Zeng, Y., 2007. Coseismic source model of the 2003 Mw6.8 Chengkung earthquake, Taiwan, determined from GPS measurements. *J. Geophys. Res.* 112, B06422.
- Chlieh, M., Avouac, J.-P., Hjørleifsdóttir, V., Song, T.-R.A., Ji, C., Sieh, K., Sladen, A., Hebert, H., Prawirodirdjo, L., Bock, Y., Galetzka, J., 2007. Coseismic slip and afterslip of the great Mw9.15 Sumatra–Andaman earthquake of 2004. *Bull. Seismol. Soc. Am.* 97, S152–S173.
- Choy, G.L., Boatwright, J.L., 1995. Global patterns of radiated seismic energy and apparent stress. *J. Geophys. Res.* 100, 18205–18228.
- Chuang, R.Y., Miller, M.M., Chen, Y.-G., Chen, H.-Y., Shyu, J.B.H., Yu, S.-B., Rubin, C.M., Sieh, K., Chung, L.-H., 2012. Interseismic deformation and earthquake hazard along the southernmost Longitudinal Valley fault, eastern Taiwan. *Bull. Seismol. Soc. Am.* 102, 1569–1582.
- Craig, T.J., Copley, A., Jackson, J., 2014. A reassessment of outer-rise seismicity and its implications for the mechanics of oceanic lithosphere. *Geophys. J. Int.* 197, 63–89.
- Craig, T.J., Heyburn, R., 2015. An enigmatic earthquake in the continental mantle lithosphere of stable North America. *Earth Planet. Sci. Lett.* 425, 12–23.
- Dalguer, L.A., Miyake, H., Day, S.M., Irikura, K., 2008. Surface rupturing and buried dynamic-rupture models calibrated with statistical observations of past earthquakes. *Bull. Seismol. Soc. Am.* 98, 1147–1161.
- Das, S., Scholz, C.H., 1983. Why large earthquakes do not nucleate at shallow depths. *Nature* 305, 621–623.
- DeMets, C., Gordon, R.G., Argus, D.F., 2010. Geologically current plate motions. *Geophys. J. Int.* 181, 1–80.
- Devlin, S., Isacks, B.L., Pritchard, M.E., Barnhart, W.D., Lohman, R.B., 2012. Depths and focal mechanisms of crustal earthquakes in the central Andes determined from teleseismic waveform analysis and InSAR. *Tectonics* 31, TC2002.
- Dogliani, C., Barba, S.C., Carminati, E., Riguzzi, F., 2011. Role of the brittle-ductile transition on fault activation. *Phys. Earth Planet. Inter.* 184, 160–171.
- Doser, D.I., Kanamori, H., 1986. Depth of seismicity in the Imperial Valley region (1977–1983) and its relationship to heat flow, crustal structure and the October 15, 1979, earthquake. *J. Geophys. Res.* 91, 675–688.
- Dziewonski, A.M., Chou, T.-A., Woodhouse, J.H., 1981. Determination of earthquake source parameters from waveform data for studies of global and regional seismicity. *Phys. Earth Planet. Inter.* 86, 2825–2852.
- Eakin, D.H., McIntosh, K.D., Avendonk, H.J.A.V., Lavier, L., Lester, R., Liu, C.-S., Lee, C.-S., 2014. Crustal-scale seismic profiles across the Manila subduction zone: the transition from intraoceanic subduction to incipient collision. *J. Geophys. Res.* 119, 1–17.
- Fujiwara, H., Kawai, S., Aoi, S., Morikawa, N., Senna, S., Kudo, N., Ooi, M., Hao, K.X., Wakamatsu, K., Ishikawa, Y., Okumura, T., Ishii, S.K., Ishikawa, Y., Okumura, T., Ishii, T., Matsushima, S., Hayakawa, Y., Toyama, N., Narita, A., 2009. Technical Reports on National Seismic Hazard Maps for Japan. National Research Institute for Earth Science and Disaster Prevention, Japan, p. 528.
- Gourley, J.R., Byrne, T., Chan, Y.-C., Wu, F., Rau, R.-J., 2007. Fault geometries illuminated from seismicity in central Taiwan: implications for crustal scale structural boundaries in the northern Central Range. *Tectonophysics* 445, 168–185.
- Hanks, T.C., Kanamori, H., 1979. A moment magnitude scale. *J. Geophys. Res.* 84, 2348–2350.
- Hashimoto, C., Noda, A., Sagiya, T., Matsu'ura, M., 2009. Interplate seismic zones along the Kuril–Japan trench inferred from GPS data inversion. *Nat. Geosci.* 2, 141–144.
- Heuret, A., Lallemand, S., Funicello, F., Piromallo, C., Faccenna, C., 2011. Physical characteristics of subduction interface type tectonic zones revisited. *Geochem. Geophys. Geosyst.* 12, Q01004.
- Hillers, G., Wesnousky, S.G., 2008. Scaling relations of strike-slip earthquakes with different slip-rate-dependent properties at depth. *Bull. Seismol. Soc. Am.* 98, 1085–1101.
- Hippchen, S., Hyndman, R.D., 2008. Thermal and structural models of the Sumatra subduction zone: implications for the megathrust seismic zone. *J. Geophys. Res.* 113, B12103.
- Ho, C.-S., 1986. A synthesis of the geologic evolution of Taiwan. *Tectonophysics* 125, 1–16.
- Hsu, S.-K., Yeh, Y.-C., Lo, C.-L., Lin, A.T., Doo, W.-B., 2008. Link between crustal magnetization and earthquakes in Taiwan. *Terr. Atmos. Ocean. Sci.* 19, 445–450.
- Hsu, S.-K., Yeh, Y.-C., Sibuet, J.-C., Doo, W.-B., Tsai, C.-H., 2013. A mega-splay fault system and tsunami hazard in the southern Ryukyu subduction zone. *Earth Planet. Sci. Lett.* 362, 99–107.
- Hsu, Y.-J., Ando, M., Yu, S.-B., Simons, M., 2012. The potential for a great earthquake along the southernmost Ryukyu subduction zone. *Geophys. Res. Lett.* 39, L14302.
- Hu, J.-C., Angelier, J., Yu, S.-B., 1997. An interpretation of the active deformation of southern Taiwan based on numerical simulation and GPS studies. *Tectonophysics* 274, 145–169.
- Hu, J.-C., Cheng, L.-W., Chen, H.-Y., Wu, Y.-M., Lee, J.-C., Chen, Y.-G., Lin, K.-C., Rau, R.-J., Kuo-Chen, H., Chen, H.-H., Yu, S.-B., Angelier, J., 2007. Coseismic deformation revealed by inversion of strong motion and GPS data: the 2003 Chengkung earthquake in eastern Taiwan. *Geophys. J. Int.* 169, 667–674.
- Huang, H.-H., Wu, Y.-M., Song, X., Chang, C.-H., Lee, S.-J., Chang, T.-M., Hsieh, H.-H., 2014. Joint Vp and Vs tomography of Taiwan: implications for subduction-collision orogeny. *Earth Planet. Sci. Lett.* 392, 177–191.
- Huang, S.-Y., Rubin, C.M., Chen, Y.-G., Liu, H.-C., 2007. Prehistoric earthquakes along the Shanchiao fault, Taipei Basin, northern Taiwan. *J. Asian Earth Sci.* 31, 176–265.
- Huang, W.J., Johnson, K.M., Fukuda, J., Yu, S.B., 2010. Insights into active tectonics of eastern Taiwan from analyses of geodetic and geologic data. *J. Geophys. Res.* 115, B03413.
- Hutton, K., Woessner, J., Hauksson, E., 2010. Earthquake monitoring in southern California for seventy-seven years (1932–2008). *Bull. Seismol. Soc. Am.* 100, 423–446.
- Ito, K., 1990. Regional variations of the cutoff depth of seismicity in the crust and their relation to heat flow and large inland-earthquakes. *J. Phys. Earth* 38, 223–250.
- Ito, K., 1999. Seismogenic layer, reflective lower crust, surface heat flow and large inland earthquakes. *Tectonophysics* 306, 423–433.
- Kagawa, T., Irikura, K., Somerville, P.G., 2004. Differences in ground motion and fault rupture process between the surface and buried rupture earthquakes. *Earth Planets Space* 56, 3–14.
- Kanamori, H., Anderson, D.L., 1975. Theoretical basis of some empirical relations in seismology. *Bull. Seismol. Soc. Am.* 65, 1073–1095.
- Kanamori, H., Lee, W.H., Ma, K.F., 2012. The 1909 Taipei earthquake—implication for seismic hazard in Taipei. *Geophys. J. Int.* 191, 126–146.
- Kao, H., 1998. Can great earthquakes occur in the southernmost Ryukyu Arc – Taiwan region? *Terr. Atmos. Ocean. Sci.* 9, 487–508.
- Kao, H., Chen, W.-P., 1991. Earthquakes along the Ryukyu–Kyushu arc: strain segmentation, lateral compression, and the thermomechanical state of the plate interface. *J. Geophys. Res.* 96, 21,443–421,485.
- Kao, H., Chen, W.-P., 2000. The Chi-Chi earthquake sequence: active, out-of-sequence thrust faulting in Taiwan. *Science* 288, 2346–2349.
- Kao, H., Huang, G.-C., Liu, C.-S., 2000. Transition from oblique subduction to collision in the northern Luzon arc-Taiwan region: constraints from bathymetry and seismic observations. *J. Geophys. Res.* 105, 3059–3080.
- Kao, H., Shen, S.-S., Ma, K.-F., 1998. Transition from oblique subduction to collision: earthquakes in the southernmost Ryukyu arc-Taiwan region. *J. Geophys. Res.* 103, 7211–7229.
- Kim, K.-H., Chiu, J.-M., Pujol, J., Chen, K.-C., Huang, B.-S., Yeh, Y.-H., Shen, P., 2005. Three-dimensional VP and VS structural models associated with the active subduction and collision tectonics in the Taiwan region. *Geophys. J. Int.* 162, 204–220.
- Kostrov, V., 1974. Seismic moment and energy of earthquakes, and seismic flow of rock. *Izv. Acad. Sci. USSR Phys. Solid Earth* 1, 23–40.
- Kuo-Chen, H., Wu, F.T., Jenkins, D.M., Mechie, J., Roecker, S.W., Wang, C.Y., Huang, B.S., 2012a. Seismic evidence for the α - β quartz transition beneath Taiwan from Vp/Vs tomography. *Geophys. Res. Lett.* 39, L22302.
- Kuo-Chen, H., Wu, F.T., Roecker, S.W., 2012b. Three-dimensional P velocity structures of the lithosphere beneath Taiwan from the analysis of TAIGER and related seismic data sets. *J. Geophys. Res.* 117, B06306.
- Kuo-Chen, H., Wu, Y.-M., Chang, C.-H., Hu, J.-C., Chen, W.-S., 2004. Relocation of eastern Taiwan earthquakes and tectonic implications. *Terr. Atmos. Ocean. Sci.* 15, 647–666.
- Kuo-Chen, H., Wu, Y.-M., Chen, Y.-G., Chen, R.-Y., 2007. 2003 Mw6.8 Chengkung earthquake and its related seismicogenic structures. *J. Asian Earth Sci.* 31, 332–339.
- Lallemand, S., Theunissen, T., Schnürle, P., Lee, C.-S., Font, Y., 2013. Indentation of the Philippine Sea plate by the Eurasia plate in Taiwan: details from recent marine seismological experiments. *Tectonophysics* 594, 60–79.
- Lay, T., Kanamori, H., 1980. Earthquake doublets in the Solomon Islands. *Phys. Earth Planet. Inter.* 21, 283–304.
- Lee, C.-T., 2004. Active Faults and Seismic Hazards in West Central Taiwan, International Conference in Commemoration of 5th Anniversary of the 1999 Chi-Chi Earthquake, Taiwan, p. 27.
- Lee, J.-C., Angelier, J., Chu, H.-T., Hu, J.-C., Jeng, F.-S., Rau, R.-J., 2003. Active fault creep variations in Chihshang, Taiwan, revealed by creep meter monitoring, 1998–2001. *J. Geophys. Res.* 108, 2528.
- Lee, J.-C., Angelier, J., Chu, H.T., Jeng, F.-S., 2001. Continuous monitoring of an active fault in a plate suture zone: a creepmeter study of the Chihshang fault, eastern Taiwan. *Tectonophysics* 333, 219–240.
- Lee, S.-J., Chen, H.-W., Huang, B.-S., 2008a. Simulations of strong ground motion and 3D amplification effect in the Taipei Basin by using a composite grid finite-difference method. *Bull. Seismol. Soc. Am.* 98, 1229–1242.
- Lee, S.-J., Chen, H.-W., Liu, Q., Komatitsch, D., Huang, B.-S., Tromp, J., 2008b. Three-dimensional simulations of seismic-wave propagation in the Taipei basin with realistic topography based upon the spectral-element method. *Bull. Seismol. Soc. Am.* 98, 253–264.
- Lester, R., Avendonk, H.J.A.V., McIntosh, K., Lavier, L., Liu, C.-S., Wang, T.K., Wu, F.T., 2014. Rifting and magmatism in the northeastern South China Sea from wide-angle tomography and seismic reflection imaging. *J. Geophys. Res.* 119, 2305–2323.
- Lester, R., McIntosh, K.D., VanAvendonk, H.J.A., Lavier, L., Liu, C.-S., Wang, T.-K., 2013. Crustal accretion in the Manila trench accretionary wedge at the transition from subduction to mountain-building in Taiwan. *Earth Planet. Sci. Lett.* 375, 430–440.
- Liao, Y.-C., Hsu, S.-K., Chang, C.-H., Doo, W.-B., Ho, M.-Y., Lo, C.-L., Lee, C.-S., 2008. Seismic tomography off SW Taiwan: a joint inversion from OBS and onshore data of 2006 Pingtung aftershocks. *Terr. Atmos. Ocean. Sci.* 19, 729–741.

- Lin, A.T.-S., Liu, C.-S., Lin, C.-C., Schnurle, P., Chen, G.-Y., Liao, W.-Z., Teng, L.S., Chuang, H.-J., Wu, M.-S., 2008. Tectonic features associated with the overriding of an accretionary wedge on top of a rifted continental margin: an example from Taiwan. *Mar. Geol.* 255, 186–203.
- Lin, A.T.-S., Watts, A.B., 2002. Origin of the West Taiwan basin by orogenic loading and flexure of a rifted continental margin. *J. Geophys. Res.* 107 (ETG 2-1–ETG 2-19).
- Lin, A.T.-S., Yao, B., Hsu, S.-K., Liu, C.-S., Huang, C.-Y., 2009. Tectonic features of the incipient arc-continent collision zone of Taiwan: implications for seismicity. *Tectonophysics* 479, 28–42.
- Lin, C.-C., Lin, A.T.-S., Liu, C.-S., Horng, C.-S., Chen, G.-Y., Wang, Y., 2013. Canyon-infilling and gas hydrate occurrences in the frontal fold of the offshore accretionary wedge off southern Taiwan. *Mar. Geophys. Res.* 35, 21–35.
- Lin, C.-H., 2001. Taiwan earthquake: a proposed stress-focusing, heel shaped model. *Bull. Seismol. Soc. Am.* 91, 1053–1061.
- Lin, C.-H., Roecker, S.W., 1993. Deep earthquakes beneath central Taiwan: mantle shearing in an arc-continent collision. *Tectonics* 12:745–755. <http://dx.doi.org/10.1029/1092TC02812>.
- Ma, K.-F., Liang, W.-T., 2008. Preface to the 2006 Pingtung earthquake doublet special issue. *Terr. Atmos. Ocean. Sci.* 19 (I–III).
- Ma, K.-F., Song, T.-R.A., 2004. Thermo-mechanical structure beneath young orogenic belt of Taiwan. *Tectonophysics* 388, 21–31.
- Ma, K.-F., Wang, J.-H., Zhao, D., 1996. Three-dimensional seismic velocity structure of the crust and uppermost mantle beneath Taiwan. *J. Phys. Earth* 44, 85–105.
- Magistrale, H., 2002. Relative contributions of crustal temperature and composition to controlling the depth of earthquakes in Southern California. *Geophys. Res. Lett.* 29, 1447.
- McIntosh, K., Nakamura, Y., Wang, T.-K., Shih, R.-C., Chen, A., Liu, C.-S., 2005. Crustal-scale seismic profiles across Taiwan and the western Philippine Sea. *Tectonophysics* 401, 23–54.
- McKenzie, D., Jackson, J., Priestley, K., 2005. Thermal structure of oceanic and continental lithosphere. *Earth Planet. Sci. Lett.* 233, 337–349.
- Miksat, J., Müller, T., Wenzel, F., 2008. Simulating three-dimensional seismograms in 2.5-dimensional structures by combining two-dimensional finite difference modelling and ray tracing. *Geophys. J. Int.* 174, 309–315.
- Miller, C.K., Furlong, K.P., 1988. Thermal-mechanical controls on seismicity depth distributions in the San Andreas Fault Zone. *Geophys. Res. Lett.* 15, 1429–1432.
- Mouyen, M., Cattin, R., Masson, F., 2010. Seismic cycle stress change in western Taiwan over the last 270 years. *Geophys. Res. Lett.* 37, L03306.
- Nazareth, J.J., Hauksson, E., 2004. The seismogenic thickness of the southern California crust. *Bull. Seismol. Soc. Am.* 94, 940–960.
- Newman, A.V., Schwartz, S.Y., Gonzalez, V., DeShon, H.R., Protti, J.M., Dorma, L.M., 2002. Along-strike variability in the seismogenic zone below Nicoya Peninsula, Costa Rica. *Geophys. Res. Lett.* 29 (38-31–38-34).
- Noda, H., Lapusta, N., 2013. Stable creeping fault segments can become destructive as a result of dynamic weakening. *Nature* 493, 518–521.
- Oleskevich, D.A., Hyndman, R.D., Wang, K., 1999. The updip and downdip limits to great subduction earthquakes: Thermal and structural models of Cascadia, south Alaska, SW Japan, and Chile. *J. Geophys. Res.* 104, 14965–14991.
- Omuralieva, A.M., Hasegawa, A., Matsuzawa, T., Nakajima, J., Okada, T., 2012. Lateral variation of the cutoff depth of shallow earthquakes beneath the Japan Islands and its implications for seismogenesis. *Tectonophysics* 518–612, 93–105.
- Pacheco, J.F., Sykes, L.R., Scholz, C.H., 1993. Nature of seismic coupling along simple plate boundaries of the subduction type. *J. Geophys. Res.* 98, 14133–14159.
- Power, M., Chiou, B., Abrahamson, N., Bozorgnia, Y., Shantz, T., Roblee, C., 2008. An overview of the NGA project. *Earthquake Spectra* 24, 3–21.
- Press, W., Teukolsky, S.A., Vetterling, V.T., Flannery, B.P., 1992. *Numerical Recipes in Fortran 77: The Art of Scientific Computing*, second ed. Cambridge University Press, Cambridge.
- Prieto, G., Shearer, P.M., Vernon, F.L., Kilb, D., 2004. Earthquake source scaling and self-similarity estimation from stacking P and S spectra. *J. Geophys. Res.* 109, B08310.
- Rau, R.-J., Wu, F.T., 1995. Tomographic imaging of lithospheric structures under Taiwan. *Earth Planet. Sci. Lett.* 133, 517–532.
- Reasenber, P.A., 1999. Foreshock occurrence before large earthquakes. *J. Geophys. Res.* 104, 4755–4768.
- Richards-Dinger, K., Shearer, P., 2000. Earthquake locations in southern California obtained using source-specific station terms. *J. Geophys. Res.* 105, 10939–10960.
- Rolandone, F., Bürgmann, R., Nadeau, R.M., 2004. The evolution of the seismic-aseismic transition during the earthquake cycle: constraints from the time-dependent depth distribution of aftershocks. *Geophys. Res. Lett.* 31, L23610.
- Rydelek, P.A., Sacks, I.S., 1989. Testing the completeness of earthquake catalogues and the hypothesis of self-similarity. *Nature* 337, 251–253.
- Scholz, C.H., 1998. Earthquakes and friction laws. *Nature* 391, 37–42.
- Schorlemmer, D., Neri, G., Wiemer, S., Mostaccio, A., 2003. Stability and significance tests for b-value anomalies: example from the Tyrrhenian Sea. *Geophys. Res. Lett.* 30, 1835.
- Schwartz, S.Y., DeShon, H.R., 2007. Distinct updip limits to geodetic locking and microseismicity at the northern Costa Rica seismogenic zone: evidence for two mechanical transitions. In: Dixon, T.H., Moore, J.C. (Eds.), *The Seismogenic Zone of Subduction Thrust Faults*, Columbia Univ. Press, New York, pp. 576–599.
- Seno, T., 2005. Variation of downdip limit of the seismogenic zone near the Japanese islands: implications for the serpentinization mechanism of the forearc mantle wedge. *Earth Planet. Sci. Lett.* 231, 249–262.
- Shaw, B.E., 2013. Earthquake surface slip-length data is fit by constant stress drop and is useful for seismic hazard analysis. *Bull. Seismol. Soc. Am.* 103, 876–893.
- Shaw, B.E., Wesnousky, S.G., 2008. Slip-length scaling in large earthquakes: the role of deep-penetrating slip below the seismogenic layer. *Bull. Seismol. Soc. Am.* 98, 1633–1641.
- Shin, T.-C., Teng, T.-L., 2001. An overview of the 1999 Chi-Chi, Taiwan, earthquake. *Bull. Seismol. Soc. Am.* 91, 895–913.
- Shyu, J.B.H., Sieh, K., Chen, Y.-G., Liu, C.-S., 2005a. The neotectonic architecture of Taiwan and its implications for future large earthquakes. *J. Geophys. Res.* 110, B08402.
- Shyu, J.B.H., Sieh, K., Chung, L.-H., Chen, Y.-G., 2005b. Tnadem suturing and disarticulation of the Taiwan orogen revealed by its neotectonic elements. *Earth Planet. Sci. Lett.* 233, 167–177.
- Sibson, R.H., 1974. Frictional constraints on thrust, wrench and normal faults. *Nature* 249, 542–544.
- Sibson, R.H., 1982. Fault zone models, heat flow, and the depth distribution of earthquakes in the continental crust of the United States. *Bull. Seismol. Soc. Am.* 72, 151–163.
- Sibson, R.H., 1984. Roughness at the base of the seismogenic zone: contributing factors. *J. Geophys. Res.* 89, 5791–5799.
- Sibson, R.H., 1986. Earthquakes and rock deformation in crustal fault zones. *Annu. Rev. Earth Planet. Sci.* 14, 149–175.
- Smith-Konter, B.R., Sandwell, D.T., Shearer, P., 2011. Locking depths estimated from geodesy and seismology along the San Andreas Fault system: implications for seismic moment release. *J. Geophys. Res.* 116, B06401.
- Somerville, P.G., 2003. Magnitude scaling of the near fault rupture directivity pulse. *Phys. Earth Planet. Inter.* 137, 201–212.
- Taira, T., Silver, P.G., Niu, F., Nadeau, R.M., 2008. Detecting seismogenic stress evolution and constraining fault zone rheology in the San Andreas Fault following the 2004 Parkfield earthquake. *J. Geophys. Res.* 113, B03303.
- Tanaka, A., Ishikawa, Y., 2002. Temperature distribution and focal depth in the crust of the northeastern Japan. *Earth Planets Space* 54, 1109–1113.
- Tanaka, A., Yamano, M., Yano, Y., Sasada, M., 2004. Geothermal gradient and heat flow data in and around Japan (I): appraisal of heat flow from geothermal gradient data. *Earth Planets Space* 56, 1191–1194.
- Theunissen, T., Lallemand, S., Font, Y., Gautier, S., Lee, C.-S., Liang, W.-T., Wu, F., Berthet, T., 2012. Crustal deformation at the southernmost part of the Ryukyu subduction (East Taiwan) as revealed by new marine seismic experiments. *Tectonophysics* 578, 10–30.
- Thomas, M.Y., Avouac, J.-P., Champenois, J., Lee, J.-C., Kuo, L.-C., 2014. Spatiotemporal evolution of seismic and aseismic slip on the Longitudinal Valley Fault, Taiwan. *J. Geophys. Res.* 119, 5114–5139.
- Tilmann, F.J., Craig, T.J., Grevemeyer, I., Suwargadi, B., Kopp, H., Flueh, E., 2010. The updip seismic/aseismic transition of the Sumatra megathrust illuminated by aftershocks of the 2004 Aceh-Andaman and 2005 Nias events. *Geophys. J. Int.* 181, 1261–1274.
- Triep, E.G., Sykes, L.R., 1997. Frequency of occurrence of moderate to great earthquakes in intracontinental regions: implications for changes in stress, earthquake prediction, and hazards assessments. *J. Geophys. Res.* 102, 9923–9948.
- Tsai, Y.-B., 1985. A study of disastrous earthquakes in Taiwan, 1683–1895. *Bull. Inst. Earth Sci. Acad. Sin.* 5, 1–44.
- Tse, S.T., Rice, J.R., 1986. Crustal earthquake instability in relation to the depth variation of frictional slip properties. *J. Geophys. Res.* 91, 9452–9472.
- Um, J., Thurber, C., 1987. A fast algorithm for two-point seismic ray tracing. *Bull. Seismol. Soc. Am.* 77, 972–986.
- Uski, M., Tiira, T., Grad, M., Yliniemi, J., 2012. Crustal seismic structure and depth distribution of earthquakes in the Archean Kuusamo region, Fennoscandian Shield. *J. Geodyn.* 53, 61–80.
- Wang, C.-Y., Chiu, J.-D., Lin, L.-A., 2001. The detection of three active faults on the Taoyuan terrace, northwestern Taiwan by shallow reflection seismics. *Terr. Atmos. Ocean. Sci.* 12, 599–614.
- Wang, C.-Y., Kuo, S.-Y., Shyu, W.-L., Hsiao, J.-W., 2003. Investigating near-surface structures under the Changhua Fault, West-central Taiwan by the reflection seismic method. *Terr. Atmos. Ocean. Sci.* 14, 343–367.
- Wang, C.-Y., Li, C.-L., Lee, H.-C., 2004. Constructing subsurface structures of the Chelungpu fault to investigate mechanisms leading to abnormally large ruptures during the 1999 Chi-Chi earthquake, Taiwan. *Geophys. Res. Lett.* 31, L02608.
- Wang, C.-Y., Li, C.-L., Su, F.-C., Leu, M.-T., Wu, M.-S., Lai, S.-H., Chen, C.-C., 2002. Structural mapping of the 1999 Chi-Chi earthquake fault, Taiwan by seismic reflection methods. *Terr. Atmos. Ocean. Sci.* 13, 211–226.
- Wang, H.-L., Zhu, L., Chen, H.-W., 2010a. Moho depth variation in Taiwan from teleseismic receiver functions. *J. Asian Earth Sci.* 37, 286–291.
- Wang, J.-C., Wang, J.-H., Shieh, C.-F., Yeh, Y.-H., 2010b. Static stress transfer between the Chinshan and Shanchiao Faults in the Taipei Metropolitan Area. *Terr. Atmos. Ocean. Sci.* 21, 515–527.
- Wang, J.-H., 1998. Studies of earthquake seismology in Taiwan during the 1897–1996 period. *J. Geol. Soc. China* 41, 291–336.
- Wang, J.-H., 2008. Urban seismology in the Taipei Metropolitan area: review and prospective. *Terr. Atmos. Ocean. Sci.* 19, 213–233.
- Wang, J.-H., Chen, K.-C., Lee, S.-J., Huang, W.-G., 2011. The 15 April 1909 Taipei earthquake. *Terr. Atmos. Ocean. Sci.* 22, 91–96.
- Wang, J.-H., Chen, K.-C., Lee, T.-Q., 1994. The depth distribution of shallow earthquakes in Taiwan. *J. Geol. Soc. China* 37, 125–142.
- Wells, D.L., Coppersmith, K.J., 1994. New empirical relationships among magnitude, rupture length, rupture width, rupture area, and surface displacement. *Bull. Seismol. Soc. Am.* 84, 974–1002.
- Wessel, P., Smith, W.M.F., 1998. New improved version of generic mapping tools released. *EOS Trans. AGU* 79, 579.
- Wiemer, S., Wyss, M., 2000. Minimum magnitude of completeness in earthquake catalogs: examples from Alaska, the western United States, and Japan. *Bull. Seismol. Soc. Am.* 90, 859–869.
- Wiens, D.A., Stein, S., 1983. Age dependence of oceanic intraplate seismicity and implications for lithospheric evolution. *J. Geophys. Res.* 88, 6455–6468.
- Williams, C.F., 1996. Temperature and the seismic/aseismic transition: observations from the 1992 Landers earthquake. *Geophys. Res. Lett.* 23, 2029–2032.

- Woessner, J., Schorlemmer, D., Wiemer, S., Mai, P.M., 2006. Spatial correlation of aftershock locations and on-fault main shock properties. *J. Geophys. Res.* 111, B08301.
- Woessner, J., Wiemer, S., 2005. Assessing the quality of earthquake catalogues: estimating the magnitude of completeness and its uncertainty. *Bull. Seismol. Soc. Am.* 95, 684–698.
- Wu, F.T., Rau, R.-J., 1998. Seismotectonics and identification of potential seismic source zones in Taiwan. *Terr. Atmos. Ocean. Sci.* 9, 739–754.
- Wu, W.-N., Kao, H., Hsu, S.-K., Lo, C.-L., Chen, H.-W., 2010. Spatial variation of the crustal stress field along the Ryukyu-Taiwan-Luzon convergent boundary. *J. Geophys. Res.* 115, B11401.
- Wu, W.-N., Zhao, L., Wu, Y.-M., 2013. Empirical relationships between aftershock zone dimensions and moment magnitudes for plate boundary earthquakes in Taiwan. *Bull. Seismol. Soc. Am.* 103, 424–436.
- Wu, Y.-M., Chang, C.-H., Hsiao, N.-C., Wu, F.T., 2003. Relocation of the 1998 Ruyli, Taiwan, earthquake sequence using three-dimensions velocity structure with stations corrections. *Terr. Atmos. Ocean. Sci.* 14, 421–430.
- Wu, Y.-M., Chen, Y.-G., Chang, C.-H., Chung, L.-H., Teng, T.L., Wu, F.T., Wu, C.-F., 2006a. Seismogenic structure in a tectonic suture zone: with new constraints from 2006 Mw6.1 Taitung earthquake. *Geophys. Res. Lett.* 33, L22305.
- Wu, Y.-M., Chen, Y.-G., Shin, T.C., Kuo-Chen, H., Hou, C.S., Hu, J.C., Chang, C.H., Wu, C.F., Teng, T.L., 2006b. Coseismic vs. interseismic ground deformations, faults rupture inversion and segmentation revealed by 2003 Mw6.8 Chengkung earthquake in eastern Taiwan. *Geophys. Res. Lett.* 33, L02312.
- Wu, Y.-M., Shyu, J.B.H., Chang, C.-H., Zhao, L., Nakamura, M., Hsu, S.-K., 2009a. Improved seismic tomography offshore northeastern Taiwan: implications for subduction and collision processes between Taiwan and the southernmost Ryukyu. *Geophys. J. Int.* 178, 1042–1054.
- Wu, Y.-M., Zhao, L., Chang, C.-H., Hsiao, N.-C., Chen, Y.-G., Hsu, S.-K., 2009b. Relocation of the 2006 Pingtung earthquake sequence and seismotectonics in Southern Taiwan. *Tectonophysics* 479, 19–27.
- Wu, Y.-M., Zhao, L., Chang, C.-H., Hsu, Y.-J., 2008. Focal mechanism determination in Taiwan by genetic algorithm. *Bull. Seismol. Soc. Am.* 98, 651–661.
- Yamanaka, Y., Kikuchi, M., 2004. Asperity map along the subduction zone in northeastern Japan inferred from regional seismic data. *J. Geophys. Res.* 109, B07307.
- Yang, W., Hauksson, E., Shearer, P.M., 2012. Computing a large refined catalog of focal mechanisms for Southern California (1981–2010): temporal stability of the style of faulting. *Bull. Seismol. Soc. Am.* 102, 1179–1194.
- Yen, Y.-T., Ma, K.-F., 2011. Source-scaling relationship for M4.6–8.9 earthquakes, specifically for earthquakes in the collision zone of Taiwan. *Bull. Seismol. Soc. Am.* 101, 464–481.
- Yu, S.-B., Chen, H.-Y., Kuo, L.-C., 1997. Velocity field of GPS stations in the Taiwan area. *Tectonophysics* 274, 41–59.
- Yu, S.-B., Kuo, L.-C., 2001. Present-day crustal motion along the Longitudinal Valley fault, eastern Taiwan. *Tectonophysics* 333, 199–217.
- Yu, S.-B., Liu, C.-C., 1989. Fault creep on the central segment of the Longitudinal Valley fault, eastern Taiwan. *Proc. Geol. Soc. China* 32, 209–231.
- Zhu, J., Sun, Z., Kopp, H., Qiu, X., Xu, H., Li, S., Zhan, W., 2013. Segmentation of the Manila subduction system from migrated multichannel seismics and wedge taper analysis. *Mar. Geophys. Res.* 34, 379–391.